



HAL
open science

Enhancement of the thermoelastic component of the photoacoustic signal of silicon membranes coated with a thin TiO₂ film

D. K. Markushev, D. D. Markushev, S Aleksić, D Pantić, S Galović, D Lukić,
Jose Ordonez-Miranda

► To cite this version:

D. K. Markushev, D. D. Markushev, S Aleksić, D Pantić, S Galović, et al.. Enhancement of the thermoelastic component of the photoacoustic signal of silicon membranes coated with a thin TiO₂ film. *Journal of Applied Physics*, 2022, 131 (8), pp.085105. 10.1063/5.0079902 . hal-03586560

HAL Id: hal-03586560

<https://hal.science/hal-03586560>

Submitted on 24 Feb 2022

HAL is a multi-disciplinary open access archive for the deposit and dissemination of scientific research documents, whether they are published or not. The documents may come from teaching and research institutions in France or abroad, or from public or private research centers.

L'archive ouverte pluridisciplinaire **HAL**, est destinée au dépôt et à la diffusion de documents scientifiques de niveau recherche, publiés ou non, émanant des établissements d'enseignement et de recherche français ou étrangers, des laboratoires publics ou privés.

Enhancement of the thermoelastic component of the photoacoustic signal of silicon membranes coated with a thin TiO₂ film

D. K. Markushev¹, D. D. Markushev¹, S.M. Aleksić^{2*}, D.S. Pantić²,
S.P. Galović³, D. V. Lukić¹, J. Ordonez-Miranda⁴

¹*Institute of Physics, University of Belgrade, Pregrevica 118, 11080 Belgrade-Zemun, Serbia*

²*Faculty of Electronic Engineering, University of Niš, Aleksandra Medvedeva 14, 18000 Niš, Serbia*

³*Vinča Institute of Nuclear Sciences, P.O. Box 522, 11001 Belgrade, Serbia*

⁴*Institut Pprime, CNRS, Université de Poitiers, ISAE-ENSMA, F-86962 Futuroscope Chasseneuil, France.*

*Corresponding author: sanja.aleksic@elfak.ni.ac.rs

Abstract. The reduction of the photogenerated charge carriers influence in periodically illuminated thin silicon membranes is investigated by using the experimental set-up of an open photoacoustic cell in the standard range of modulation frequencies from 20 Hz to 20 kHz. It is confirmed that the deposition of a 200nm thin film of titanium dioxide on the 30- and 50 μm silicon membrane leads to a large increase of the thermoelastic component of the photoacoustic signal, which restores the flexibility lost to the membrane under the influence of photogenerated carriers. The effect of the thermoelastic component enhancement is analyzed by observing the displacement of the tested samples along the heat propagation axis, depending on the carrier density and temperature differences on the illuminated and unilluminated sides, for different membrane thicknesses and a constant film thickness. It is found that the effect of enhancement of several orders of magnitude is more visible in thinner membranes, due to higher ratios between the film and membrane thicknesses.

Introduction

It is well known that the illumination of semiconductors with a modulated light source can generate charge carriers that cause different types of thermal responses [1-5]. There are various spectroscopic methods within photothermal sciences that can be used to analyze such thermal responses [6-12]. In our previous articles [13-15], we showed that photoacoustics (PA) is a method by which different thermal responses of semiconductors can be clearly observed under the strong influence of photogenerated carriers, by analyzing different patterns of behavior of photoacoustic signals and their components. It was observed that the influences of carriers on the thermal response are most intense in semiconductor membranes having the shape of circular plates with a thickness smaller than the sample carrier diffusion length (so-called plasma-thin samples). A strong decrease in the amplitude of the thermoelastic component and a decrease in the total phase of the photoacoustic signal was observed as a typical pattern of the PA signal behavior in the frequency domain [13,14]. In practical terms, it means that the degree of bending of the illuminated semiconductor membrane decreases under the influence of photogenerated carriers. This is a very significant effect that can affect the reliability, accuracy, and sensitivity of MEMS sensors (e.g., pressure sensors), of which silicon membranes are an integral part [15]. Among the others, the zero and span calibration shifts are the most frequent errors caused by Si membrane illumination. They may be sufficient to cause unacceptable mistakes in the sensors operation process so their avoidance is the ultimate manufacturing goal.

One very important question also arises: is there a way to significantly reduce the influence of photogenerated carriers on the bending degree of illuminated semiconductor membranes? Our research shows that this can be done by coating the silicon membranes with

a thin transparent film on the membrane illuminated side. Such film should be made of a material that does not generate charge carriers at the light source wavelength, transparent to allow direct membrane excitation, having the thickness relatively large enough to be visible in photoacoustic measurements. Titanium dioxide (TiO_2), with which we already have experience in working with plasma-thick samples [16,17], appears to be a good thin film candidate.

Here, we measure and analyze photoacoustic signals (amplitudes and phases) generated by the single- (silicon membranes 30- and 50 μm thick) and two-layer samples (30- and 50 μm thick silicon membrane substrate + thin TiO_2 film of constant 200 nm thickness) and monitor the behavior of their thermoelastic components. This is done by using an open photoacoustic cell operating in the transmission configuration with modulation frequencies from 20 Hz to 20 kHz. The relationship between the PA signal thermoelastic component and the thermoelastic bending degree is studied, by using the sample displacement as a parameter involved in the applied theoretical model.

Theoretical background

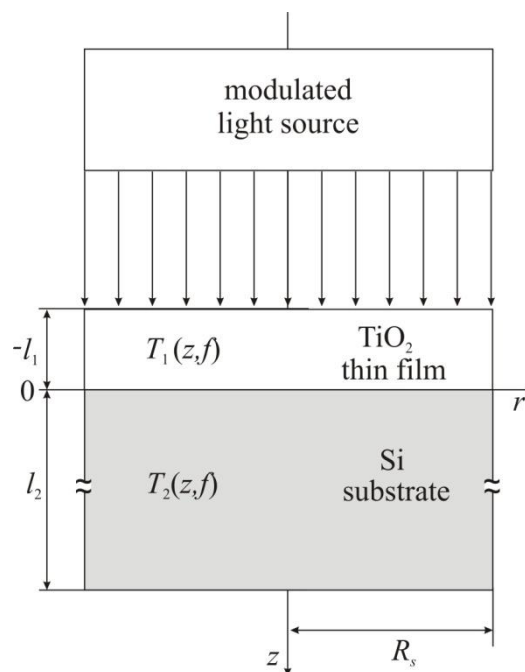


Figure 1. The simplest scheme of the two-layer sample irradiated by modulated light source. l_1 and l_2 ($l_1 \ll l_2$) are the thicknesses of the thin film (TiO_2) and substrate (Si), respectively. R_s is the sample radius, $T_1(z,f)$ is the temperature in the thin film and $T_2(z,f)$ is the temperature in the substrate.

The thermal response of a semiconductor sample illuminated by a modulated light source is a consequence of several processes. The first one is the process of light absorption resulting in an increase in the internal energy which leads to the sample heating and temperature gradient formation. Due to the mentioned gradient formation, the thermal diffusion process starts to transfer heat through the sample periodically changing its temperature in the bulk and on its surfaces. At the same time, the temperature difference on the illuminated and non-illuminated side of the sample results in the process of sample periodic, so-called thermoelastic bending. In addition, the generation of free carriers on the illuminated side of the sample results in their diffusion through the semiconductor material, periodically changing their concentrations within and on its surfaces. Different concentrations of carriers

on different sides of the sample lead to its periodic bending process, so-called plasma-elastic bending.

All of the mentioned processes are incorporated in the theoretical model of composite pistons [18,19], the well known model of photoacoustics. Although this model is basically made for single-layer samples consisting of pure arbitrary material, it can be easily adapted to multi-layer structures as well. The typical scheme used for thermal response analysis of a two-layer sample (Si substrate + TiO₂ thin film) irradiated from one side by the modulated light source is presented in Figure 1. The presented scheme is used for the explanation of 1D heat transfer along the heat flow axes parallel to the sample thickness. The samples used in the presented investigation has cylindrical symmetry so cylindrical coordinates are a reasonable choice and heat transfer is assumed to take place along the z -axes.

The photoacoustic response of the two-layer sample irradiated with the modulated light source (Figure 1) [16,17,20] can be theoretically described by the total PA signal $\delta p_{\text{total}}(f)$ defined with the simple equation [13, 14]:

$$\delta p_{\text{total}}(f) = \delta p_{\text{TD}}(f) + \delta p_{\text{TE}}(f) + \delta p_{\text{PE}}(f), \quad (1)$$

where f is the modulation frequency, and $\delta p_{\text{TD}}(f)$, $\delta p_{\text{TE}}(f)$, and $\delta p_{\text{PE}}(f)$ are the thermal diffusion (TD), thermoelastic (TE) and plasma elastic (PE) PA signal components, respectively. Using a simple 1D theoretical model [13,16,17,20] these components can be written as:

$$\delta p_{\text{TD}}(f) = \frac{p_0 \gamma_g T_2(l_2, f)}{\sigma_g l_c T_0}, \quad (2)$$

$$\delta p_c(f) = \frac{\gamma P_0}{V_0} \int_0^{R_s} 2\pi r U_{z,c}(r, z) dr, \quad c = \text{TE, PE} \quad (3)$$

where γ is the adiabatic constant, p_0 and T_0 are the equilibrium pressure and temperature of the air in microphone, $\sigma_g = (1+i)/\mu_g$, μ_g is the thermal diffusion length of the air; l_c is the PA cell length, $T_2(l_2, f)$ is the dynamic temperature variation at the substrate rear (non-illuminated) surface [18-20], V_0 is the photoacoustic cell volume, and $U_{z,c}(r, z)$ is the sample displacement along the z -axes.

The $U_{z,c}(r, z)$ of the two-layer sample at the back surface, $z = l_2$, important in a transmission photoacoustic measurements, can be written in a general form as [16,17,20]:

$$U_{z,c}(r, z) = \frac{C_c}{2} (R_s^2 - r^2), \quad c = \text{TE, PE}, \quad (4)$$

where R_s is the sample radius and

$$C_{\text{TE}} = 6 \frac{A_1 + A_2 + E_1 E_2 [\alpha_{T1} l_2 (2M_{T1} - l_2 N_{T1}) + \alpha_{T2} l_1 (2M_{T2} + l_1 N_{T2})]}{E_1^2 l_1^4 + E_2^2 l_2^4 + 2E_2 E_1 l_2 l_1 (2l_2^2 + 3l_2 l_1 + 2l_1^2)}, \quad (5.a)$$

$$C_{PE} = 6d_n E_2 \frac{[E_1 l_1 (2M_n + l_1 N_n) + E_2 l_2 (2M_n - l_2 N_n)]}{E_2 l_2^4 + E_1 l_1^4 + 2E_2 E_1 l_2 l_1 (2l_2^2 + 3l_2 l_1 + 2l_1^2)}. \quad (5.b)$$

Here $A_1 = E_1 l_1 (2M_{T1} + l_1 N_{T1}) \alpha_{T1}$, $A_2 = E_2 l_2 (2M_{T2} - l_2 N_{T2}) \alpha_{T2}$, E_1 and E_2 are the Young's modulus of the film and substrate, respectively, d_n is the coefficient of electronic deformation and M_{T1} , M_{T2} , M_n , N_{T1} , N_{T2} and N_n are defined as [16,17,20]

$$M_{T1} = \int_{-l_1}^0 z T_1(z, f) dz, \quad M_{T2} = \int_0^{l_2} z T_2(z, f) dz, \quad M_n = \int_0^{l_2} z \delta n_p(z, f) dz, \quad (6)$$

$$N_{T1} = \int_{-l_1}^0 T_1(z, f) dz, \quad N_{T2} = \int_0^{l_2} T_2(z, f) dz, \quad N_n = \int_0^{l_2} \delta n_p(z, f) dz, \quad (7)$$

where $T_1(z, f)$ is the temperature in the thin film and $T_2(z, f)$ is the temperature in the substrate and $\delta n_p(z, f)$ is the photogenerated minority carrier density. The M_{T1} , and M_{T2} are the first moments of the temperature change, and the M_n is the first moment of the photogenerated minority carriers change along the z -axis. The N_{T1} and N_{T2} are the average temperature changes and N_n is the average photogenerated minority carriers change along the z -axes.

In the case of one-layer sample (Figure 1, substrate only) Eqs.(1-7) reduces to [13,14,18]

$$\delta p_{total}^*(f) = \delta p_{TD}^*(f) + \delta p_{TE}^*(f) + \delta p_{PE}^*(f), \quad (8)$$

$$\delta p_{TD}^*(f) = \frac{p_0 \gamma_g T_2(l_2, f)}{\sigma_g l_c T_0}, \quad (9)$$

$$U_{z,TE}^*(r, z) = \alpha_{T2} \frac{6(R_s^2 - r^2)}{l_2^3} M_{T2}, \quad M_{T2} = \int_0^{l_2} \left(z - \frac{l_2}{2}\right) T_2(z, f) dz \quad (10.a)$$

$$U_{z,PE}^*(r, z) = d_n \frac{6(R_s^2 - r^2)}{l_2^3} M_n, \quad M_n = \int_0^{l_2} \left(z - \frac{l_2}{2}\right) \delta n_p(z, f) dz \quad (10.b)$$

$$\delta p_{TE}^*(f) = \alpha_{T2} \frac{\gamma p_0}{V_0} \frac{3\pi R_s^4}{l_2^3} \int_0^{l_2} \left(z - \frac{l_2}{2}\right) T_2(z, f) dz, \quad (11)$$

and

$$\delta p_{PE}^*(f) = d_n \frac{\gamma p_0}{V_0} \frac{3\pi R_s^4}{l_2^3} \int_0^{l_2} \left(z - \frac{l_2}{2}\right) \delta n_p(z, f) dz. \quad (12)$$

Results and Discussion

To check the influence of thin films on the bending degree of illuminated silicon membranes, we measured the amplitude $A(f)$ and phase $\varphi(f)$ of the photoacoustic signal $S(f) = A(f)\exp[i\varphi(f)]$ as functions of the modulation frequency f within the 20Hz – 20kHz range [13,16,17]. Measurements were carried out for two thicknesses of membranes (50 μm and 30 μm) with (S_{exp}) and without (S_{exp}^*) the 200 nm-thick TiO_2 thin film coating, illuminated with the laser diode light source having 660 nm wavelength and intensity of $I_0 = 10\text{W}/\text{m}^2$. The results of such measurements are presented in Figure 2. All substrate samples used in presented investigation are made from the same n -type Si wafer ($\langle 100 \rangle$, 3-5 Ωcm) in the form of thin circular plates (membranes) having the radius $R_s = 30$ mm. The TiO_2 thin films were deposited on Si membranes using RF sputtering technique [16].

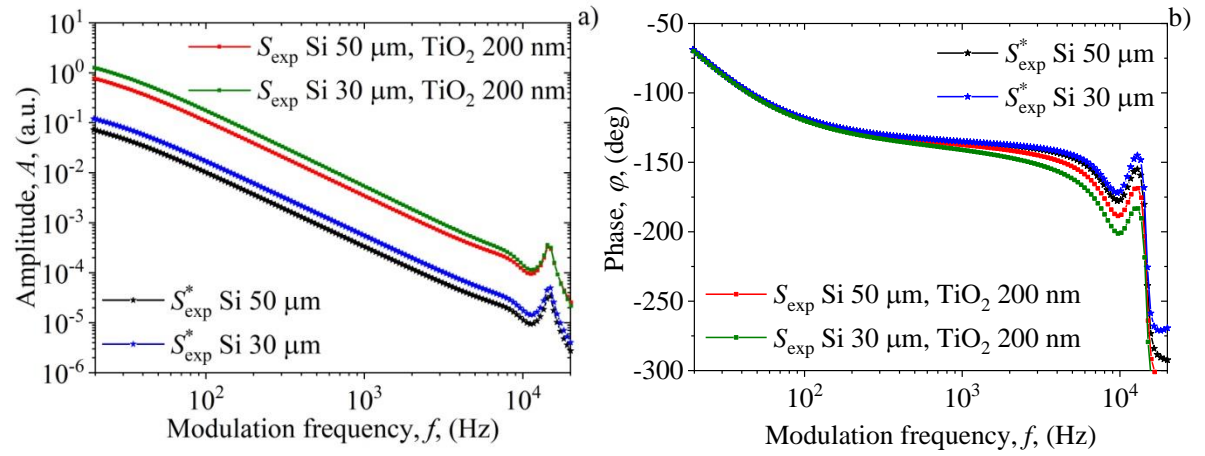


Figure 2. Experimental photoacoustic signal a) amplitude A and b) phase φ of Si membranes with $S_{\text{exp}}(f)$ and without $S_{\text{exp}}^*(f)$ thin TiO_2 film as a function of modulation frequencies f .

The amplitudes and phases of the measured photoacoustic signals $S_{\text{exp}}^*(f)$ and $S_{\text{exp}}(f)$ shown in Figures 2.a and 2.b, respectively, were obtained using an open photoacoustic cell apparatus operating in the transmission mode, described in detail in our previous articles [13,14]. All these signals are a complex combination of the “real” photoacoustic signals $\delta p_{\text{total}}^*(f)$ (Eq.(8)) and $\delta p_{\text{total}}(f)$ (Eq.(1)) that come directly from the illuminated samples and their electronic $H_e(f)$ and acoustic $H_a(f)$ deviations caused by the influence of measuring instruments [13,20] (Appendix I):

$$S_{\text{exp}}^*(f) = \delta p_{\text{total}}^*(f) H_e(f) H_a(f) \quad (13)$$

and

$$S_{\text{exp}}(f) = \delta p_{\text{total}}(f) H_e(f) H_a(f). \quad (14)$$

Table I. Basic Si and TiO_2 parameters obtained after signal correction procedure

	Si	TiO_2
β [$10^5/\text{m}$]	(2.6+0.2)	(1.8+0.4)
D_T [$10^{-6}\text{m}^2/\text{s}$]	(9.0+0.1)	(3.9+0.5)
α_T [$10^{-6}/\text{K}$]	(2.6+0.2)	(11+2)
k [W/mK]	(150+2)	(10+3)

The influence of measuring instruments can be simply described as electronic filtering (H_e) which reduces the signal amplitude in the low-frequency range, and acoustic filtering (H_a) which generates typical signal peaks at higher frequencies (Figures 3&4, Appendix I), usually recognized as shaped, or tailored, microphone frequency response [21]. The measured signals $S_{\text{exp}}^*(f)$ and $S_{\text{exp}}(f)$ are corrected by the well-known procedure of recognizing and removing H_e and H_a [13,21] in order to obtain $\delta p_{\text{total}}^*(f)$, $\delta p_{\text{total}}(f)$ and corresponding basic sample parameters: coefficient of optical absorption β , thermal diffusivity D_T , coefficient of thermal expansion α_T , thermal conductivity k . The results of such procedure are presented in Table I. They are in accordance with the literature values obtained by different methods [22-25] and our previous research [13,16]. Other important parameters, like Young's modulus of the film ($E_1 = 280$ GPa) and substrate ($E_2 = 137$ GPa), the coefficient of electronic deformation ($d_n = -9.0 \times 10^{-31}$ m³) and photogenerated carriers lifetime ($\tau = 6 \times 10^{-6}$ s) are taken from the same literature [13,16,22-25].

Based on the composite piston theory [18], obtained $\delta p_{\text{total}}^*(f)$ and $\delta p_{\text{total}}(f)$ are disassembled into three signal components – TD, TE and PE, whose amplitudes and phases are shown in Figures 3.a, c & 4a, c in the case of single-layer (Si membranes, Eqs.(8-12)), and Figures 3b, d & 4b, d in the case of two-layer systems (Si membrane + thin TiO₂ film, Eqs.(1-7)).

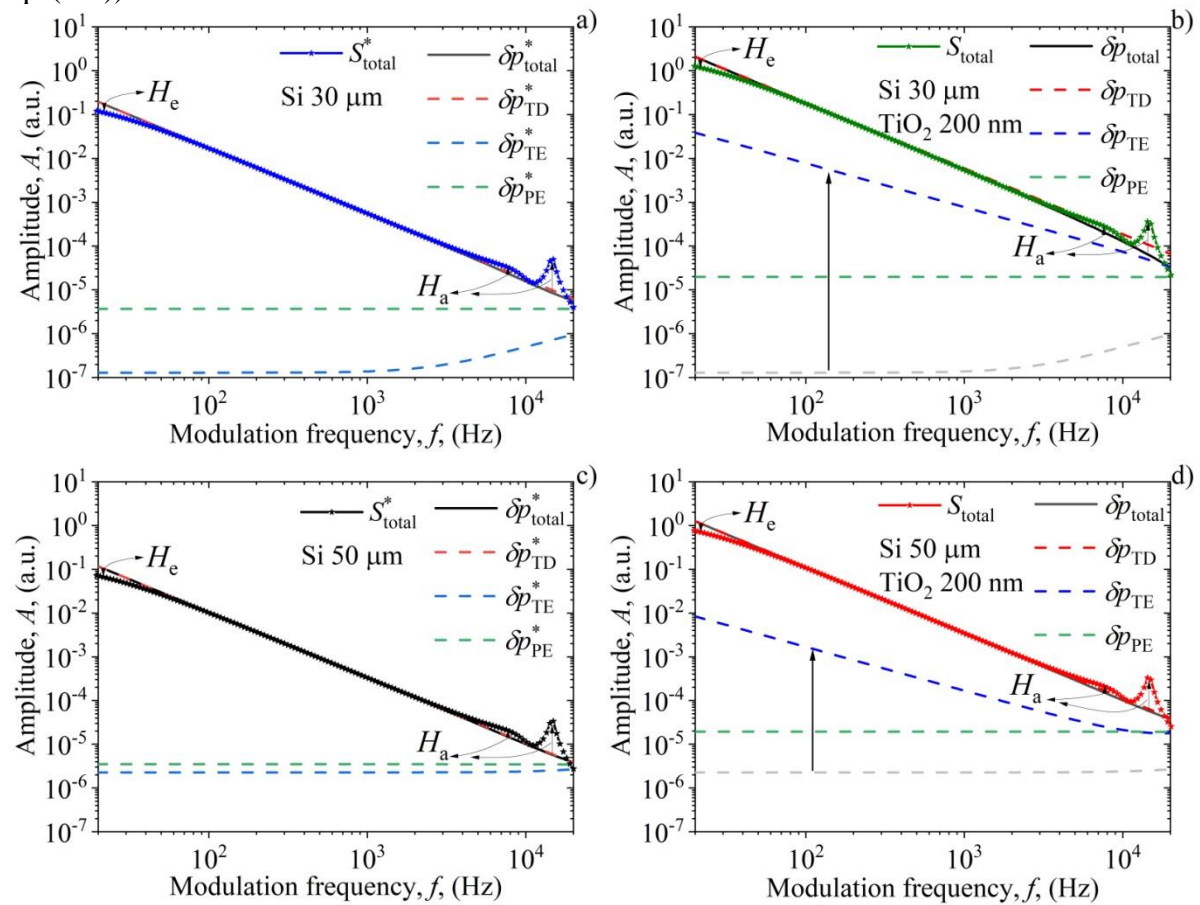
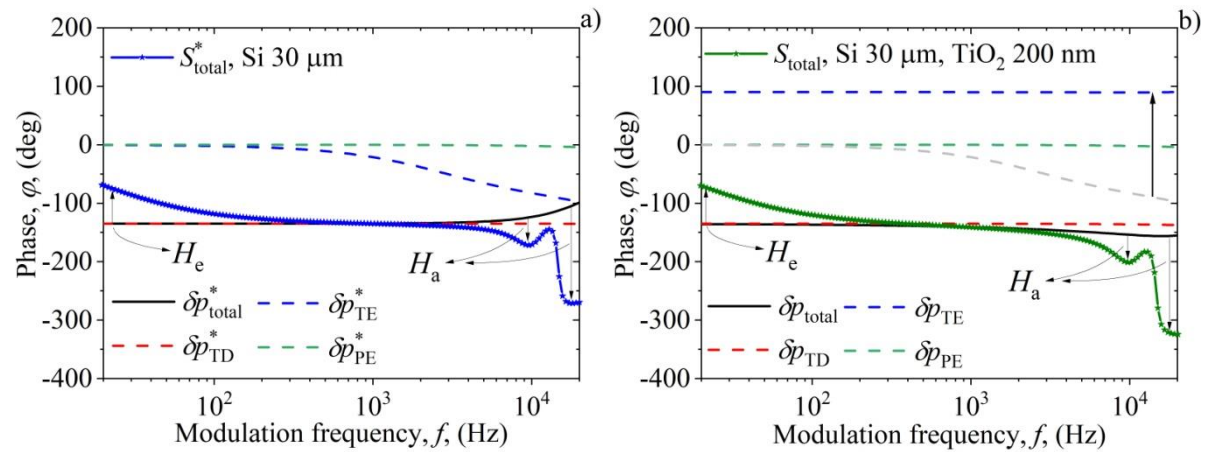


Figure 3. Experimental (asterisks) and corrected (solid line) total photoacoustic signals along with the corresponding components (dashed lines) for the amplitudes A of the Si membranes without $S_{\text{exp}}^*(f)$ (a,c) and with $S_{\text{exp}}(f)$ (b,d) a thin TiO₂ film, as functions of the modulation frequency f .

The changes in the mutual relationships of the photoacoustic signal components are clearly visible in Figures 3&4. They are caused by the deposition of a thin TiO₂ film on both membrane thicknesses. Larger mutual relationship changes are detected in the case of the thinner substrate (30 μm), where the amplitude of the total signal decreases at higher frequencies more intensely (up to 35% lower values) in the case of the two-layer system (Figure 3.b) compared to the pure silicon (Figure 3.a). In the case of the thicker substrate (50 μm) total amplitude decrease is much lower: up to 5% lower values in the case of the two-layer system (Figure 3.d) at middle frequencies compared to the pure silicon (Figure 3.c). At the same time total phase in pure silicon (Figure 4.a,c) at higher frequencies increases, but in the case of a two-layer system (Figures 4.b,d) total phase decreases. One can conclude that explained effects of the total PA amplitudes and phases behavior in frequency domain are more intense in the case of thinner substrates [13,14].

Comparing Figures 3.a,c & 3.b,d, it is obvious that the amplitude of the thermoelastic component (blue dashed line) undergoes the greatest changes: a) for pure silicon, under the action of photogenerated carriers, TE amplitude at low frequencies drops to $\sim 10^{-7}$ (Figure 3.a) and $\sim 10^{-6}$ (Figure 2.c), changing its functional dependence at higher frequencies [13,14]; b) TE amplitude of the two-layer system increases up to $\sim 10^{-1}$ (Figure 3.b) and $\sim 10^{-2}$ (Figure 3.d) at lower frequencies, decreasing in the entire frequency domain up to $\sim 10^{-4}$ (Figure 3.b) and $\sim 10^{-5}$ (Figure 2.d) at higher frequencies. For clarity, in Figures 3.b and 3.c, the thermoelastic components of the pure silicon samples are marked with dashed gray lines so that the increase in the thermoelastic component, which is indicated by arrows, should be more noticeable.

In phases (Figure 4), as in amplitudes, the thermoelastic component (blue dashed line) suffers the largest changes, which are indicated by the arrows in Figures 4.b and 4.d, where the dashed gray line represents the thermoelastic component phase of pure silicon samples (Figures 4.a and 4.c).



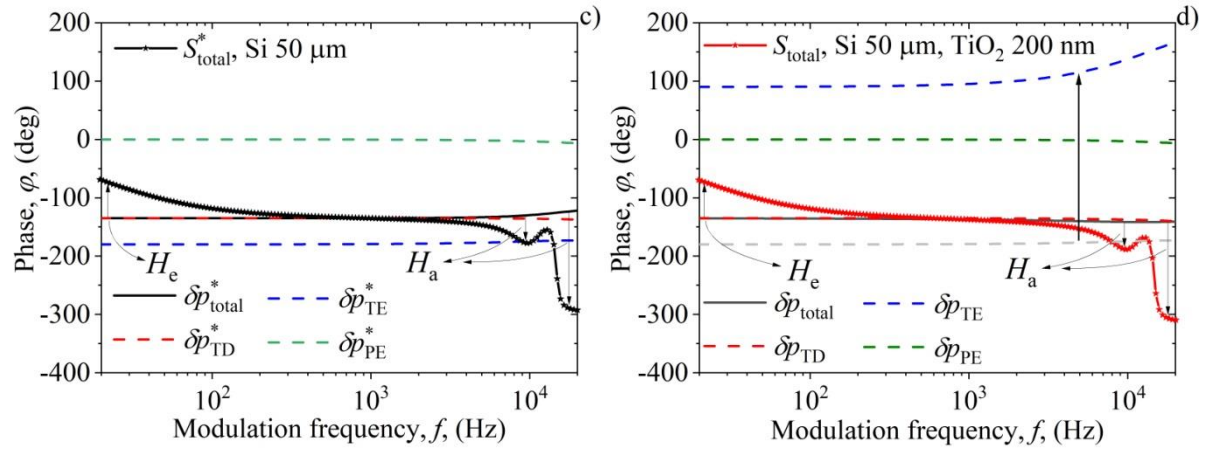


Figure 4. Experimental (asterisks) and corrected (solid line) total photoacoustic signals along with the corresponding signal components (dashed lines) for the phases φ of the Si membranes without $S_{\text{exp}}^*(f)$ (a,c) and with $S_{\text{exp}}(f)$ (b,d) a thin TiO₂ film, as functions of the modulation frequency f .

Analyzing Eqs. (3&11) one can conclude that presented thermoelastic component amplitude behavior in all cases (Figures 3) was guided by the displacements of the sample along the z -axis $U_{z,\text{TE}}(r,z)$. Following such behavior the results of $U_{z,\text{TE}}^*(r,z)$ (Eq.(10.a)) and $U_{z,\text{TE}}(r,z)$ (Eqs. (4-6)), for both substrate thicknesses, in the case of $z = l_2$ and $r = 0$ in the whole range of modulation frequencies are presented in Figure 5, where clear differences can be seen between “pure” and “coated” membranes.

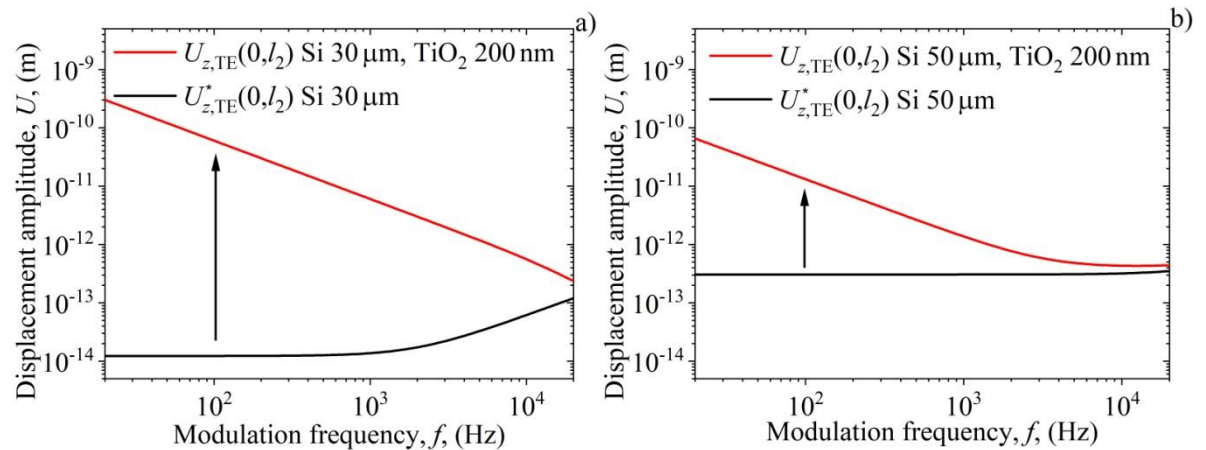


Figure 5. Thermoelastic displacements of the a) 30 μm and b) 50 μm Si membranes with $U_{z,\text{TE}}(r,z)$ and without $U_{z,\text{TE}}^*(r,z)$ a thin TiO₂ film, as functions of modulation frequency f .

In the generalized scheme, displacements of membranes of different thicknesses with and without a thin film (Figure 5) can be simply represented as in Figure 6. Regardless of the thickness of the substrate, the $U_{z,\text{TE}}^*(r,z) < U_{z,\text{TE}}(r,z)$ ratio will always apply.

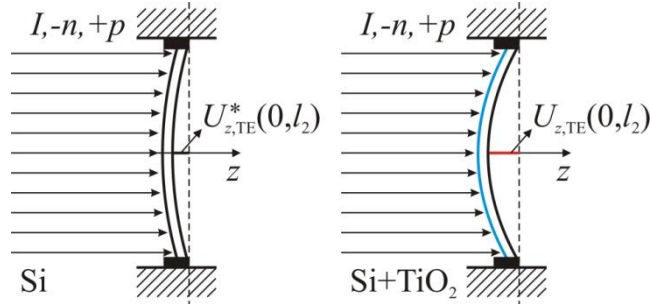


Figure 6. Schemes of the thermoelastic displacement of the irradiated Si membranes with $U_{z,TE}(r, z)$ and without $U_{z,TE}^*(r, z)$ a thin TiO_2 film (blue line), where photogenerated electrons ($-n$) and holes ($+p$) are present.

To find the cause of differences between $U_{z,TE}^*(r, z)$ and $U_{z,TE}(r, z)$ one need to analyze the changes in C_{TE} values (Eq.(5.a)). It is obvious that these changes depend on the mutual relationships between M_{T1} , and N_{T1} , and M_{T2} and N_{T2} . Changes in the first moments and/or average temperature changes can lead to the changes in C_{TE} , and thus in $U_{z,TE}(r, z)$ changes. The first moments and average temperatures depend on the temperature distribution in the sample, and temperature distribution depends on the density distribution of the photogenerated carriers. This is the reason why one can attribute all changes in $U_{z,TE}^*(r, z)$ and $U_{z,TE}(r, z)$ behaviour to changes in differences of the photogenerated carrier densities $\Delta\delta n_p^*$, $\Delta\delta n_p$, and temperatures ΔT_2^* , ΔT_2 , at the substrate surfaces (illuminated, $z=0$, and nonilluminated, $z=l_2$) defined by

$$\Delta\delta n_p^* = \delta n_p^*(0) - \delta n_p^*(l_2), \quad \Delta\delta n_p = \delta n_p(0) - \delta n_p(l_2),$$

and

$$\Delta T_2^* = T_2^*(0) - T_2^*(l_s), \quad \Delta T_2 = T_2(0) - T_2(l_s).$$

The analysis results are presented in Table II, where all carrier densities (Appendix II) and substrate temperatures (Appendix III) corresponds to the calculated sample displacements $U_{z,TE}^*(0, l_2)$ and $U_{z,TE}(0, l_2)$ (Figure 5), for both substrate thicknesses l_2 and three characteristic modulation frequencies (100-, 1000- and 20000 Hz). One must always bear in mind that $T_1(0) = T_2(0)$ (Figure 1) is one of the boundary conditions for temperature calculations (Appendix II).

The results presented in Table II show that the film deposition on substrate reduces the differences in carrier density ($\Delta\delta n_p < \Delta\delta n_p^*$) and temperatures ($\Delta T_2 < \Delta T_2^*$) on the illuminated and unilluminated sides of the sample. These reductions indicate a decrease in the influence of free carriers, i. e. an increase in the degree of bending (flexibility) which is the main goal of this work. The influence of carrier and temperature decrease on $U_{z,TE}(0, l_2)$ is larger at lower frequencies, while at higher ones, such influence is reflected through the dominant mutual relationship between M_{T2} and N_{T2} : the impact of the film becomes insignificant. Also, $U_{z,TE}(0, l_2)$ is larger for thinner substrates, which is expected, since $U_{z,TE} \propto l_2^{-3}$ (Eqs.(4),(5)&(10)).

Table II. Temperatures at sample surfaces (Illuminated and nonilluminated), their differences and ratios, together with sample displacements of Si and Si+TiO₂ at characteristic modulation frequencies.

$l_2 = 30 \mu\text{m}$						
f (Hz)	$\Delta\delta n_p^*$ (10^{18}m^{-3})	$\Delta\delta n_p$ (10^{18}m^{-3})	ΔT_2^* (10^{-10}K)	ΔT_2 (10^{-10}K)	$U_{z,\text{TE}}^*(0, l_2)$ (10^{-13}m)	$U_{z,\text{TE}}(0, l_2)$ (10^{-13}m)
100	3.08353	2.97450	-14.99	-13.573	0.1232	609.41
1000	3.08345	2.97442	-155.92	-141.16	0.1381	152.96
20000	3.05548	2.94744	-2926.2	-2636.7	1.2131	2.3370
$l_2 = 50 \mu\text{m}$						
f (Hz)	$\Delta\delta n_p^*$ (10^{18}m^{-3})	$\Delta\delta n_p$ (10^{18}m^{-3})	ΔT_2^* (10^{-10}K)	ΔT_2 (10^{-10}K)	$U_{z,\text{TE}}^*(0, l_2)$ (10^{-13}m)	$U_{z,\text{TE}}(0, l_2)$ (10^{-13}m)
100	4.90665	4.73315	-12.67	-4.21	3.065	132.52
1000	4.90637	4.73288	-138.26	-43.7	2.5486	13.4
20000	4.80161	4.63183	-1626.9	-101.3	3.3993	4.43

Conclusions

The enhancement of the thermoelastic component of the photoacoustic signal measured by using an open photoacoustic cell for plasma-thin silicon samples with a thin layer of TiO₂ has been studied. The photoacoustic theory for two-layer samples consisting of a substrate in the form of 30- and 50- μm thick Si membranes, and a 200 nm-thick TiO₂ film has been used in the data analysis. These substrate thicknesses are smaller than the diffusion length of the heat carriers, while the film is thick enough to be well visible for photoacoustic measurements. It has been found that the TiO₂ film enhances both the amplitude and phase of the thermoelastic component of the photoacoustic signal of the entire two-layer system. This enhancement is a direct consequence of the sample displacement along the heat propagation axis, such that larger displacements are obtained for the thinner substrate (30 μm). This is reasonable as the displacement of a two-layer sample is inversely proportional to the (thickness)³ of the substrate. Based on the analysis of the photogenerated carrier densities and temperature differences at the illuminated and nonilluminated sides of the samples, for three characteristic modulation frequencies, it has been shown that the displacement of two-layer samples is larger than that of the single-layer ones. The TiO₂ film, therefore, suppresses the influence of the photogenerated carriers and enhances the bending of the sample described by the thermoelastic component of the photoacoustic signal. The obtained results thus show that the loss of flexibility of Si samples induced by photogenerated carriers can be overcome by depositing a thin transparent TiO₂ film on the illuminated Si side, which can be useful for developing MEMS and the electronic industry in general.

Acknowledgments

This work was supported by the Ministry of Education, Science and Technological Development of the Republic of Serbia, within the institutional financing, contract number 451-03-09/2021-14/200017.

References

- [1] M. Kaviany, (2014). Heat transfer physics (2nd ed.). Cambridge: Cambridge University Press. [ISBN 978-1-107041783](#).
- [2] D.K. Ferry, (2013), Semiconductors, Bonds and bands, IOP Publishing Ltd, Bristol, UK
- [3] I. Lashkevych, O. Titov and Yu.G. Gurevich, Recombination and temperature distribution in semiconductors, *Semicond. Sci. Technol.* **27**, 055014 (2012)
[doi:10.1088/0268-1242/27/5/055014](#)
- [4] Volz, S. (2010). Microscale and Nanoscale Heat Transfer (Topics in Applied Physics). Springer. [ISBN 978-3642071584](#).
- [5] S.S. Li (2006) Excess Carrier Phenomenon in Semiconductors. In: S.S. Li (eds) Semiconductor Physical Electronics, Springer, New York, NY
- [6] Stephen E. Bialkowski, Nelson G.C. Astrath, Mikhail A. Proskurnin, (2019) Photothermal Spectroscopy Methods, *Chemical Analysis: A Series of Monographs on Analytical Chemistry and Its Applications* (New York: John Wiley & Sons) ISBN: 9781119279075
- [7] M. Pawlak, “Photothermal, photocarrier, and photoluminescence phenomena in semiconductors studied using spectrally resolved modulated infrared radiometry: Physics and applications”, *J. Appl. Phys.* **126**, 150902 (2019);
<https://doi.org/10.1063/1.5114719>
- [8] D. Fournier, A. C. Boccara, A. Skumanish, and N. M. Amer, “Photothermal investigation of transport in semiconductors: Theory and experiment”, *J. Appl. Phys.* **59**, 787 (1986)
<https://doi.org/10.1063/1.336599>
- [9] Yu.G. Gurevich, I. Lashkevych, "Sources of Fluxes of Energy, Heat, and Diffusion Heat in a Bipolar Semiconductor: Influence of Nonequilibrium Charge Carriers", *Int. J. Thermophys.* **34**, 341 (2013) <https://doi.org/10.1007/s10765-013-1416-0>
- [10] Yu. G. Gurevich and J. E. Velázquez-Pérez, “The role of non-equilibrium charge carriers in thermoelectric cooling *J. Appl. Phys.* **114**, 033704 (2013)
<http://dx.doi.org/10.1063/1.4813514>
- [11] Photoacoustic and Thermal Wave Phenomena in Semiconductors, edited by A. Mandelis (Elsevier, New York, 1987).
- [12] Semiconductors and Electronic Materials, Progress in Photothermal and Photoacoustic Science and Technology, edited by A. Mandelis and P. Hess, (SPIE Press, Washington, 2000).
- [13] D.K. Markushev, D.D. Markushev, S.M. Aleksic, D.S. Pantic, S.P. Galovic, D.M. Todorovic and J. Ordonez-Miranda, Experimental photoacoustic observation of the photogenerated excess carrier influence on the thermoelastic response of n-type silicon, *J. Appl. Phys.* **128**, 095103 (2020) <https://doi.org/10.1063/5.0015657>
- [14] D.K. Markushev, D.D. Markushev, S.M. Aleksic, D.S. Pantic, S.P. Galovic, D.M. Todorovic and J. Ordonez-Miranda, Effects of the photogenerated excess carriers on the thermal and elastic properties of n-type silicon excited with a modulated light source: Theoretical analysis, *J. Appl. Phys.* **126**, 185102 (2019)
<https://doi.org/10.1063/1.5100837>
- [15] D.K. Markushev, D.D. Markushev, S.P. Galovic, S.M. Aleksic, D.S. Pantic, D.M. Todorovic, “The surface recombination velocity and bulk lifetime influences on photogenerated carrier density and temperature distributions in n-type silicon excited by a frequency-modulated light source”, *Facta Univ. Ser. Electron. Energ.* **31**, 2, 313 – 328 (2018)
<https://doi.org/10.2298/FUEE1802313M>

This is the author's peer reviewed, accepted manuscript. However, the online version of record will be different from this version once it has been copyedited and typeset.
PLEASE CITE THIS ARTICLE AS DOI: 10.1063/1.50079902

- [16] D.M. Todorović, M.D. Rabasović, D.D. Markushev and M. Sarajlic, Photoacoustic elastic bending in thin film-substrate system: Experimental determination of the thin film parameters, *Journal of Applied Physics*, **116**, (2014) 053506, doi: 10.1063/1.4890346
- [17] D.M. Todorović, M.D. Rabasović, and D.D. Markushev, Photoacoustic elastic bending in thin film—Substrate system, *J. Appl. Phys.* **114**, 213510 (2013)
<https://doi.org/10.1063/1.4839835>
- [18] F.A. McDonald, G.C. Wetsel Jr, Chapter 4, Theory of Photothermal and Photoacoustic Effects in Condensed Matter, In *Physical Acoustics*, **18**, 167-277 (1988)
<https://doi.org/10.1016/B978-0-12-477918-1.50010-2>
- [19] A. Rosencwaig, “Thermal wave characterization and inspection of semiconductor materials and devices” in „Photoacoustic and Thermal Wave Phenomena in Semiconductors“, ed. A. Mandelis, (Elsevier Publishing Company, 1987), pp. 97-135
- [20] N. Jovančić, D.K. Markushev, D.D. Markushev, S.M. Aleksić, D.S. Pantić, D. Korte, M. Franko, Thermal and Elastic Characterization of Nanostructured Fe₂O₃ Polymorphs and TiO₂-Coated Fe₂O₃ Using Open Photoacoustic Cell, *Int. J. Thermophys.* **41**, 90 (2020),
<https://doi.org/10.1007/s10765-020-02669-w>
- [21] D.D. Markushev, M.D. Rabasović, D.M. Todorović, S.Galović, and S.E. Bialkowski, Photoacoustic signal and noise analysis for Si thin plate: Signal correction in frequency domain, *Rev. Sci. Instrum.* **86**, 035110 (2015),
<https://doi.org/10.1063/1.4914894>
- [22] Mohammed Hadi. Shinen, S.A.A. AlSaati, F.Z. Razooqi, Preparation of high transmittance TiO₂ thin films by sol-gel technique as antireflection coating, *J. Phys.: Conf. Ser.* **1032** (2018) 012018,
<https://doi.org/10.1088/1742-6596/1032/1/012018>
- [23] A. Kot, M. Radecka, D. Dorosz, K. Zakrzewska, Optically Active TiO₂:Er Thin Films Deposited by Magnetron Sputtering, *Materials*, **14** (2021) 4085,
<https://doi.org/10.3390/ma14154085>
- [24] I. Sta, M. Jlassi, M. Hajji, M.F. Boujmil, R. Jerbi, M. Kandyla, M. Kompitsas, and H. Ezzaouia, Structural and optical properties of TiO₂ thin films prepared by spin coating, *J. Sol-Gel Sci. Technol.* **72**, 421-427 (2014)
<https://doi.org/10.1007/s10971-014-3452-z>
- [25] <https://www.azom.com/properties.aspx?ArticleID=1179>

Appendix I. The influence of measuring instruments on the photoacoustic signal

The photoacoustic signal generated by the sample excited by the modulated light source contains various influences of the instruments used in its measurement. A detailed analysis determines that such influences arise mostly from the microphones used in measurements and accompanying electronics. These effects are reflected in signal distortion due to different types of filtering at low and high frequencies [13,21].

At low frequencies (< 1 kHz), the PA signal is distorted in a way typical for the high-pass filters: amplitude decrease and phase increases with decreasing frequencies (Figure 7). The degree of distortion is described by the cascade connection of the RC low-pass filters. Each filter corresponds to one instrument with characteristic RC values. Therefore, low-frequency filtering of photoacoustic signals is called electronic filtering described by the $H_e(f)$ function [13,21]:

$$H_e(f) = -\frac{\omega\tau_{c1}}{(1+i\omega\tau_{c1})} \times \frac{\omega\tau_{c2}}{(1+i\omega\tau_{c2})}, \quad (\text{A1})$$

where $\omega = 2\pi f$, f is the modulation frequency, $\tau_{c1} = (2\pi f_{c1})^{-1} = R_1C_1$ and $\tau_{c2} = (2\pi f_{c2})^{-1} = R_2C_2$ are the time constants and RC characteristics of the microphone (A1) and signal processing electronics (2) (usually the sound-card or lock-in).

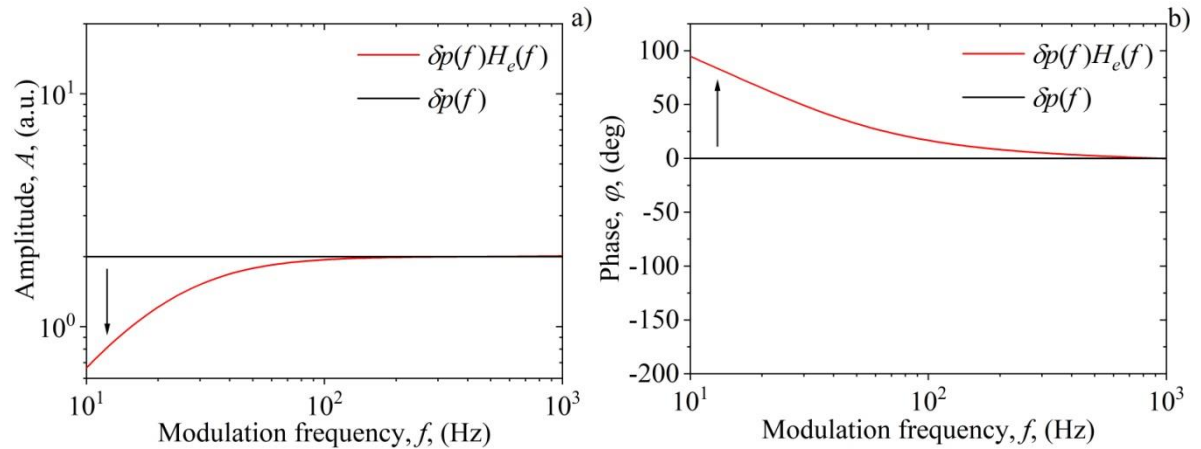


Figure 7. Typical signal distortion (red line) of the a) amplitude A and b) phase φ for modulation frequencies $f < 1$ kHz.

At high frequencies (> 1 kHz), the PA signal is distorted in a way typical for the low-pass filters: sharp jumps and falls of amplitude and phase values occur which gives typical peak structure responses (Figure 8). The size and shape of peaks with characteristic frequencies and dumping factors are described by the sum of low-frequency RCL filters. Since the peaks are a typical high-frequency microphone response caused by its acoustic characteristics, filtering in the high-frequency region is called acoustic filtering described by the function $H_a(f)$ [13,21]:

$$H_a(f) = \frac{\omega_{c3}^2}{\omega_{c3}^2 + i\delta_{c3}\omega_{c3}\omega - \omega^2} + \frac{\omega_{c4}^2}{\omega_{c4}^2 + i\delta_{c4}\omega_{c4}\omega - \omega^2}, \quad (\text{A2})$$

where δ_k is the damping factor ($k = c3, c4$), ω_{c3} is the microphone cut-off frequency and ω_{c4} is the characteristic frequency which depends on the geometry of the microphone body.

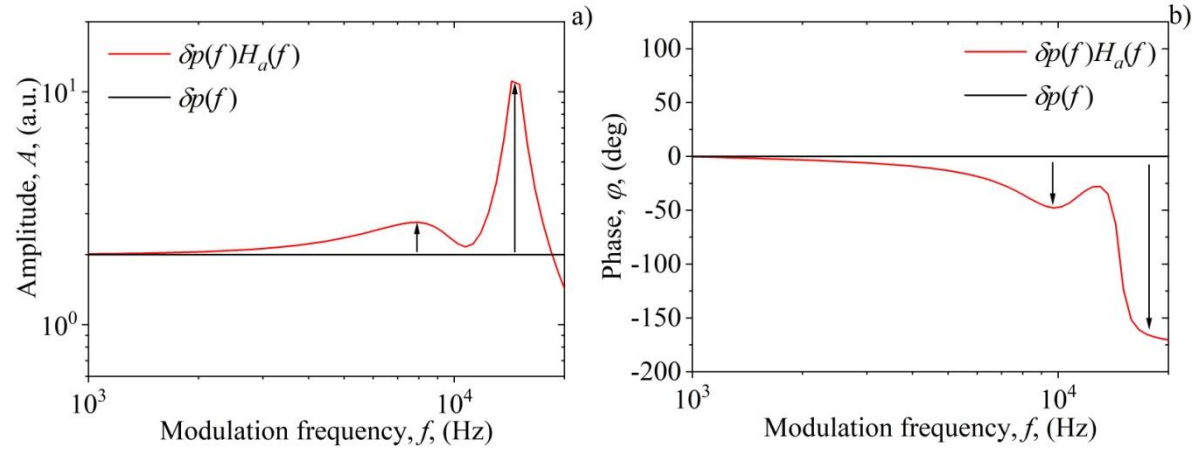


Figure 8. Typical signal distortion (red line) at high-frequencies with a) amplitude A and b) phase ϕ behavior at modulation frequencies $f > 1$ kHz.

Characteristic PA signal distortion $H_e(f)$ and $H_a(f)$ parameters calculated from our presented and previous measurements [13], used here to draw Figures 7 & 8, are presented in Table III.

Table III. Characteristic PA signal distortion H_e and H_a parameters used to obtain figures 7 & 8.

Characteristic frequency f_{c1} , (Hz)	25
Characteristic frequency f_{c2} , (Hz)	5
Characteristic frequency f_{c3} , (Hz)	9400
Characteristic frequency f_{c4} , (Hz)	14700
Damping factor δ_{c3}	0.6
Damping factor δ_{c4}	0.08

Appendix II. Periodic carrier densities in Si substrate

Within the photoacoustics, photogenerated carrier density calculations are based on the Fick's second law of diffusion, assuming that electrons and holes are generated in pairs as identical particles neglecting their electrical nature. Considering that the used Si membranes (Figure 1) are the low-level injection n -type semiconductors (minority carriers are used to explain carrier dynamics), the dynamic part of the 1D diffusion equation (important for sound wave generation) that explains carrier transport in membranes can be written in the form [13-15]:

$$\frac{d^2 \delta n_p(z, f)}{dz^2} - \frac{\delta n_p(z, f)}{L^2} = -\frac{\beta I_0}{\epsilon D_p} e^{-\beta z}, \quad (\text{B1})$$

where $L = L_p / (1 + i2\pi f \tau_p)^{1/2}$ is the complex excess carriers diffusion length, $L_p = \sqrt{D_p \tau_p}$ is the excess carrier diffusion length, i is the complex unit, $\delta n_p(z, f)$ is the

photogenerated minority (holes) dynamic density component, D_p is the holes diffusion coefficient, and τ_p is their lifetime. The solution $\delta n_p(z, f)$ of the Eq.(17) is given by [13-15]:

$$\delta n_p(z) = A_+ e^{z/L} + A_- e^{-z/L} - A e^{-\beta z}, \quad (\text{B2})$$

where $A = I_0 / (\varepsilon D_p \beta)$, and the integration constants A_{\pm} are defined by [13-15]:

$$A_{\pm} = \frac{A v_{\beta} (v_D \pm s_2) e^{\mp l_2/L} - v_D (v_{\beta} - s_2) e^{-\beta l_2}}{v_D (v_D + s_2) e^{l_2/L} - (v_D - s_2) e^{-l_2/L}}, \quad (\text{B3})$$

depending strongly on the relative ratio of the characteristic diffusion speeds $v_D = D_p / L$ and $v_{\beta} = \beta D_p$.

Appendix III. Periodic temperature distributions in the thin TiO₂ film and Si substrate

Periodic temperature distributions in the thin film (1-TiO₂) and substrate (2-Si) illuminated by the modulated light source (Figure 1) can be obtained solving the thermal-diffusion equations in the form [16,17,20]:

$$\frac{\partial^2 T_1(z, f)}{\partial z^2} - \frac{i\omega}{D_{T1}} T_1(z, f) = -\frac{1}{k_1} \beta_1 (1 - R_1) I_0 e^{-\beta_1 z}, \quad (\text{C1})$$

and

$$\frac{\partial^2 T_2(z, f)}{\partial z^2} - \sigma_2^2 T_2(z, f) = -\frac{\varepsilon_s}{k_2 \tau_2} n_p(z, f) - \frac{\beta_2 I}{k_2} \times \frac{\varepsilon - \varepsilon_s}{\varepsilon} e^{-\beta_2 z}, \quad (\text{C2})$$

where $\omega = 2\pi f$, f is the modulation frequency, I_0 is the incident light intensity, $I = (1 - R_1)(1 - R_2) e^{-\beta_1 l} I_0$, R_1 is the film reflection coefficient, R_2 is the substrate reflection coefficient, $\sigma_1 = \sqrt{i\omega / D_{T1}}$ is the film complex thermal diffusivity, D_{T1} is the film thermal diffusion coefficient, $\sigma_2 = \sqrt{i\omega / D_{T2}}$ is the substrate complex thermal diffusivity, D_{T2} is the substrate thermal diffusion coefficient, k_1 is the thin film heat conduction coefficient, k_2 is the substrate heat conduction coefficient, β_1 is the film absorption coefficient, β_2 is the substrate absorption coefficient, and $\delta n_p(z, f)$ is the photogenerated minority carrier dynamic density component (Eq.(18)).

The general solutions of Eqs.(17,18) can be written in the form [20]:

$$T_1(z, f) = A_1 e^{\sigma_1 z} + A_2 e^{-\sigma_1 z} + A_3 e^{-\beta_1 z}, \quad (\text{C3})$$

and

$$T_2(z, f) = B_1 e^{\sigma_2 z} + B_2 e^{-\sigma_2 z} + B_3 n_p(z, f) + B_4 e^{-\beta_2 z}, \quad (\text{C4})$$

where the constants A_3 , B_3 and B_4 are given as:

$$A_3 = -\frac{\beta_1 I_0 (1-R_1)}{k_1 (\beta_1^2 - \sigma_1^2)}, \quad B_3 = -\frac{\varepsilon_g}{k_2 \tau_{p2} \left(\sigma_2^2 - \frac{1}{L^2} \right)},$$

$$B_4 = -\frac{\beta_2 (1-R_1)(1-R_2) e^{-\beta_1 l_1} I_0 \left(\frac{B_3}{D_p} - \frac{\varepsilon - \varepsilon_g}{k_2} \right)}{\varepsilon (\beta_2^2 - \sigma_2^2)}.$$

Constants A_1, A_2, B_1 and B_2 can be found solving the boundary conditions [20]:

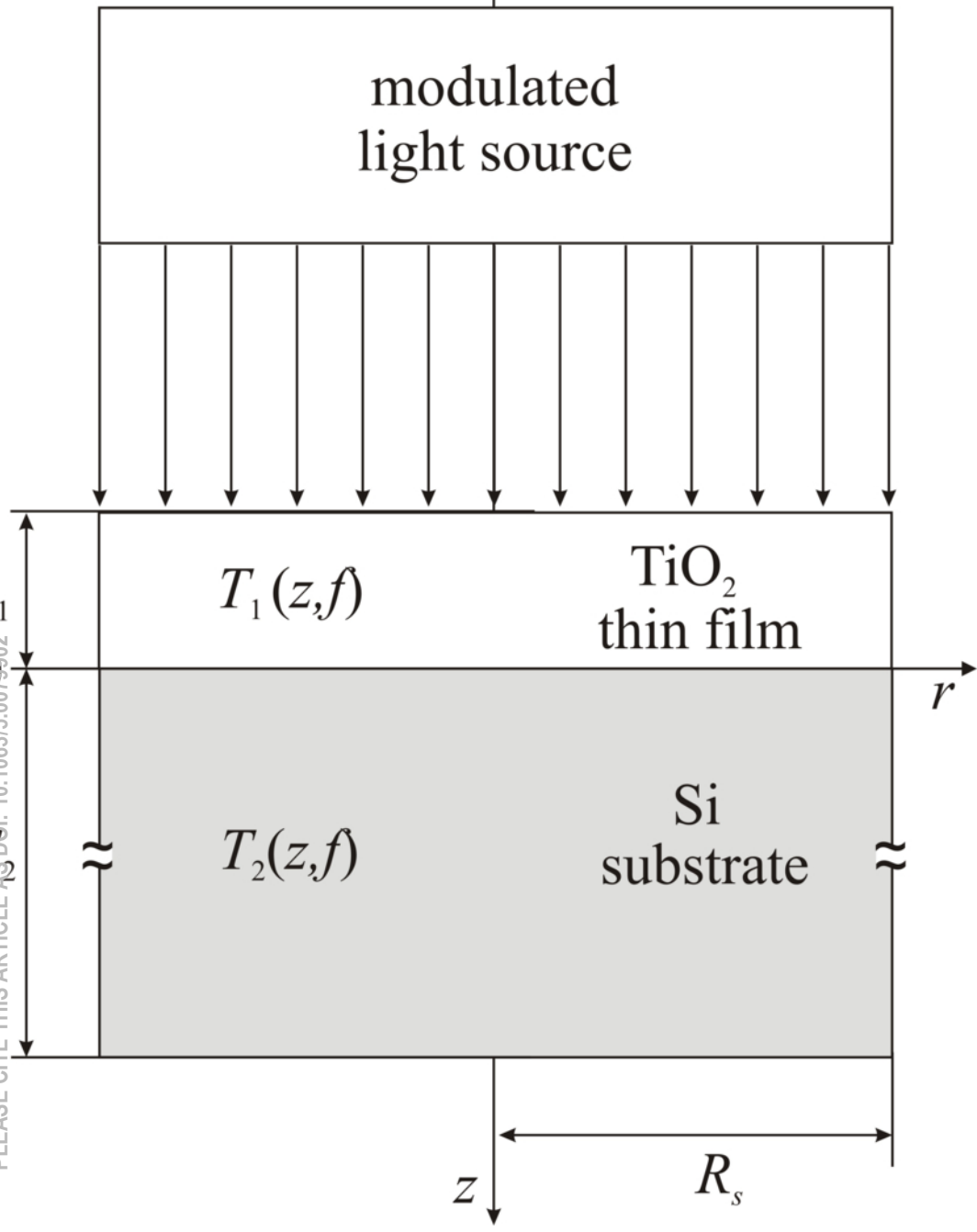
$$\begin{aligned} \text{a) } & -k_1 \frac{\partial T_1(z, f)}{\partial z} \Big|_{z=-l_1} = 0, \quad \text{b) } T_1(0, f) = T_2(0, f), \\ \text{c) } & -k_2 \frac{\partial T_2(z, f)}{\partial z} \Big|_{z=0} = s_F n_p(0, f) \varepsilon_g - k_1 \frac{\partial T_1(z, f)}{\partial z} \Big|_{z=0}, \\ \text{d) } & -k_2 \frac{\partial T_2(z, f)}{\partial z} \Big|_{z=l_2} = -s_R n_p(l_2, f) \varepsilon_g, \end{aligned} \quad (\text{C5})$$

where s_F and s_R are the substrate surface recombination speeds at the front ($z=0$) and rear ($z=l_2$) surfaces, respectively. Based on our previous investigations [13-17,20], the analysis of the two-layer optical properties shows that the multiple optical reflections can be neglected in the Si substrate [13], but must be taken into account in the case of thin TiO_2 film. This is the reason why the film reflection coefficient R_1 is calculated here using [16,17]:

$$R_1 = r_F + (1-r_F)^2 r_R \times \frac{e^{-2\beta_1 l_1}}{1-r_F r_R e^{-2\beta_1 l_1}}, \quad (\text{C6})$$

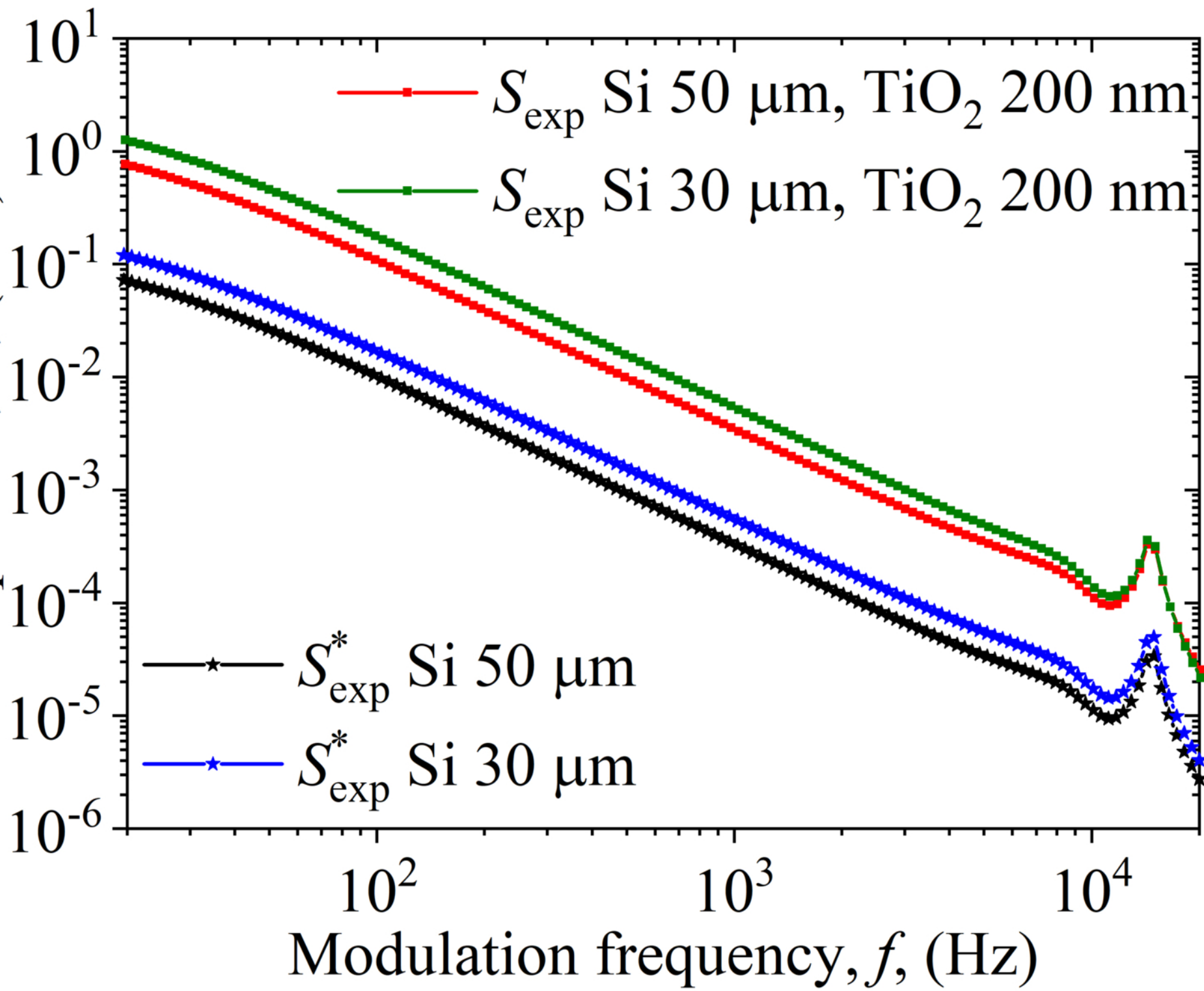
where r_F and r_R are the front and rear thin film reflectivity coefficients, respectively.

This is the author's peer reviewed, accepted manuscript. However, the online version of record will be different from this version once it has been copyedited and typeset.
PLEASE CITE THIS ARTICLE AS: [10.1063/5.0019902](https://doi.org/10.1063/5.0019902)



This is the author's peer reviewed, accepted manuscript. However, the online version of record will be different from this version once it has been copyedited and typeset.
PLEASE CITE THIS ARTICLE AS DOI: 10.1063/1.5079902

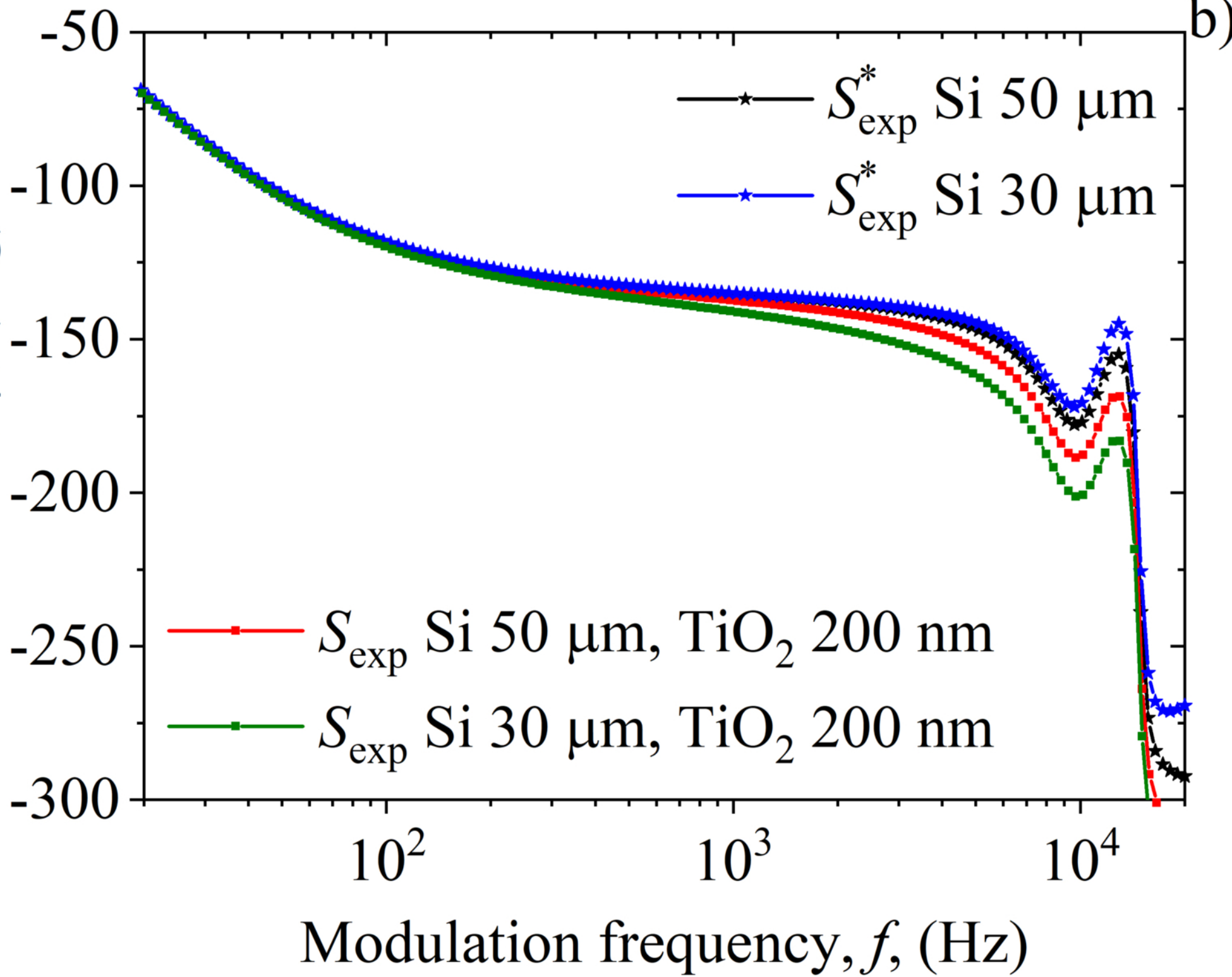
Amplitude, A , (a.u.)

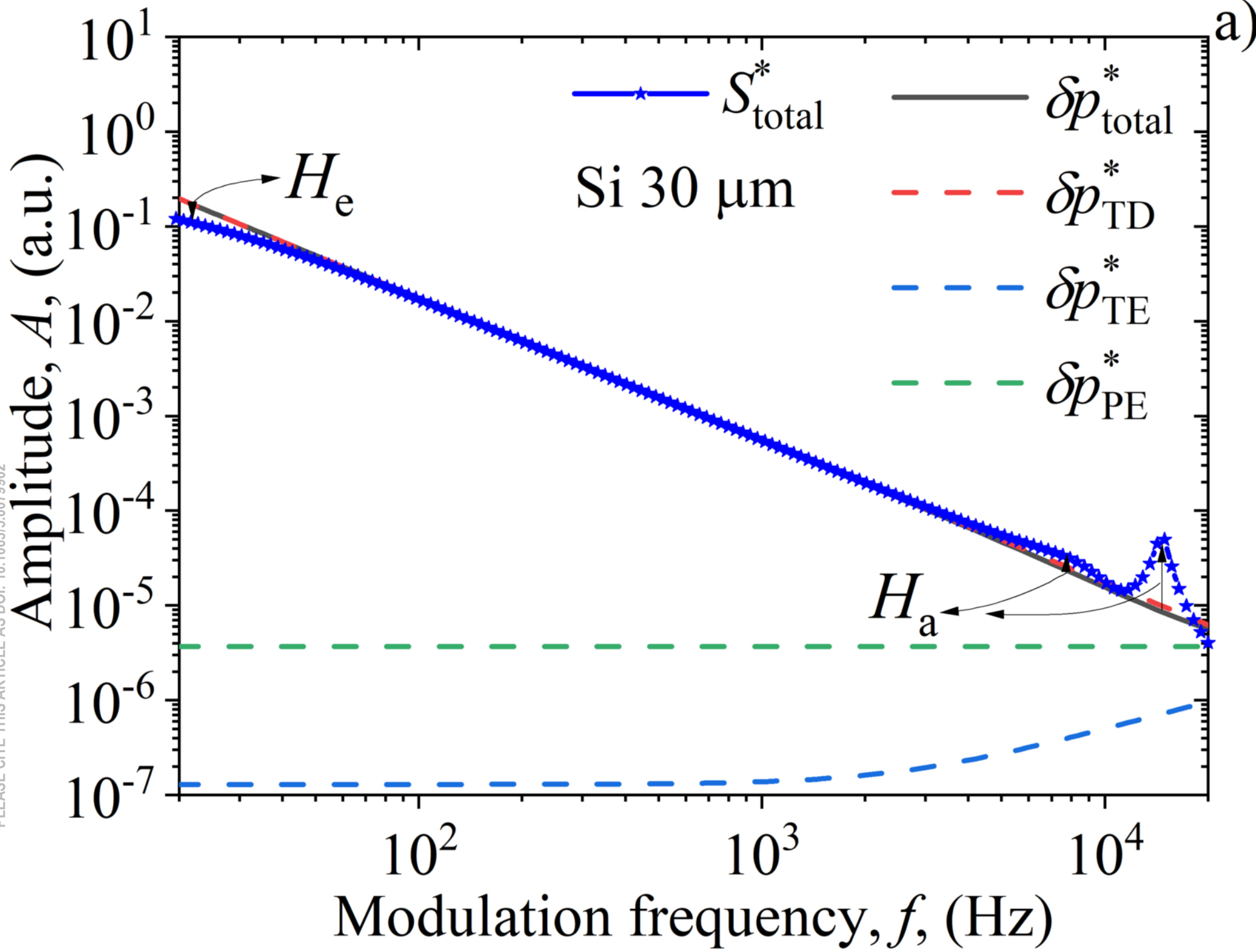


a)

This is the author's peer reviewed, accepted manuscript. However, the online version of record will be different from this version once it has been copyedited and typeset.
PLEASE CITE THIS ARTICLE AS DOI: 10.1063/1.5098802

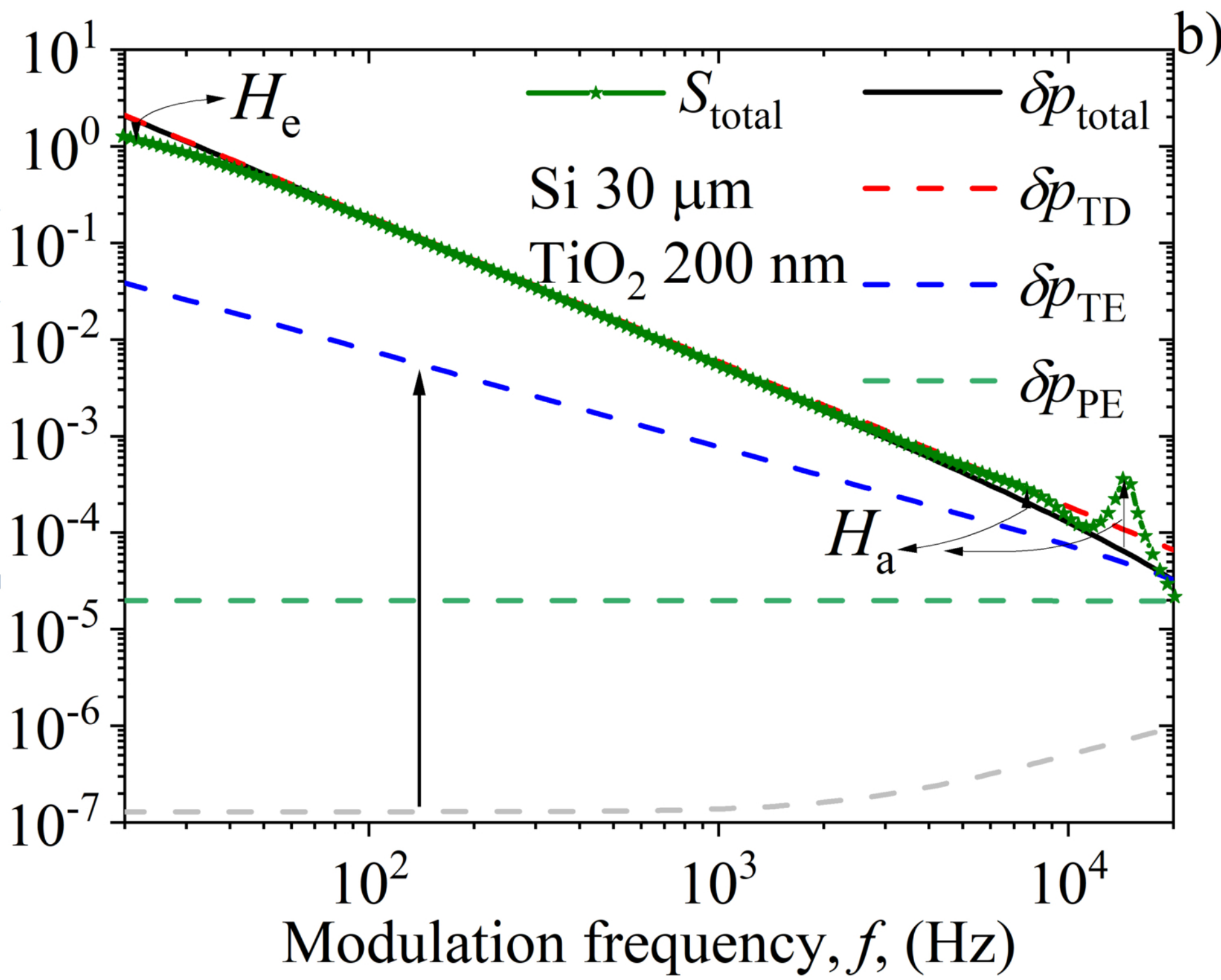
Phase, φ , (deg)





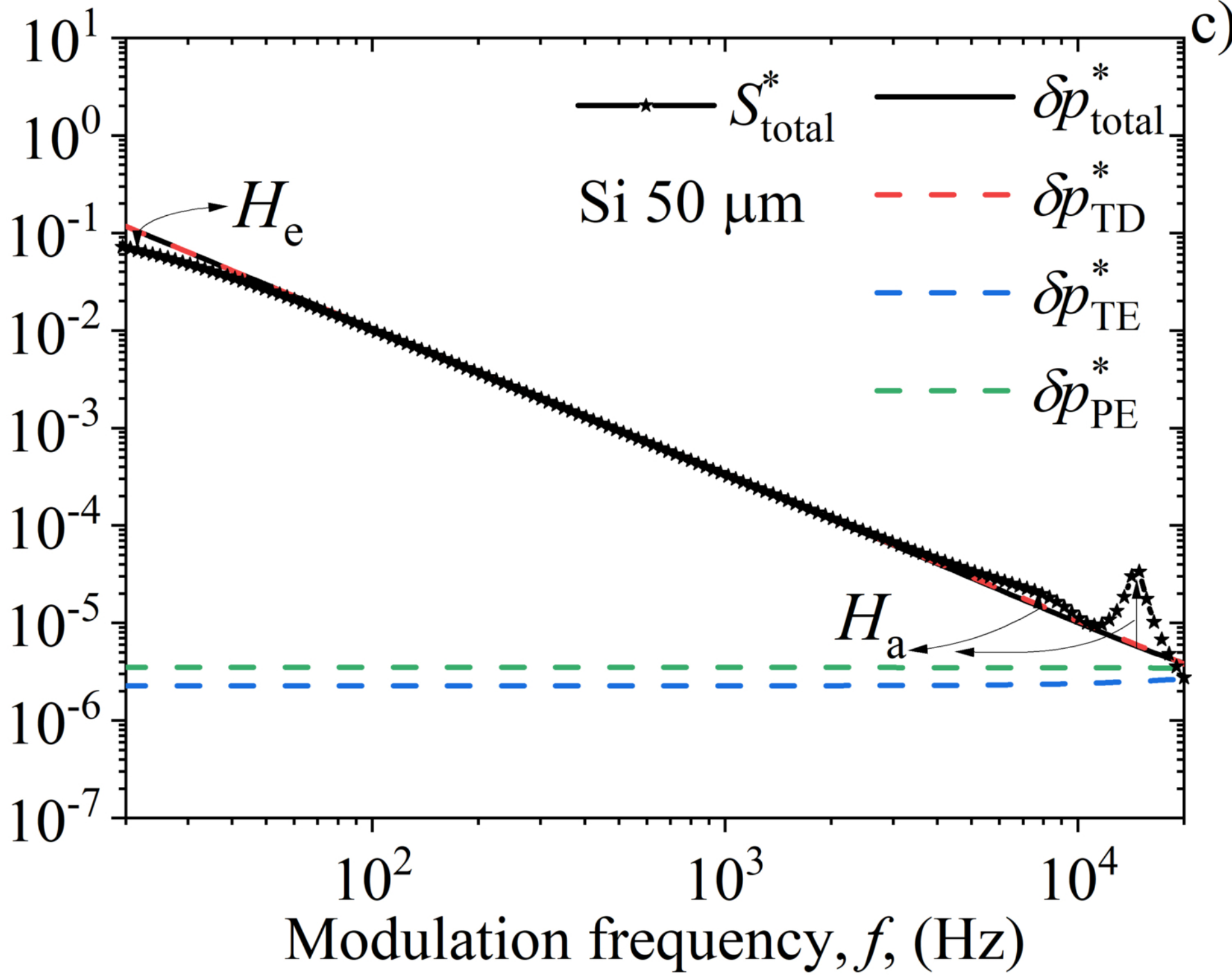
This is the author's peer reviewed, accepted manuscript. However, the online version of record will be different from this version once it has been copyedited and typeset.
PLEASE CITE THIS ARTICLE AS DOI: 10.1063/5.0079902

Amplitude, A , (a.u.)



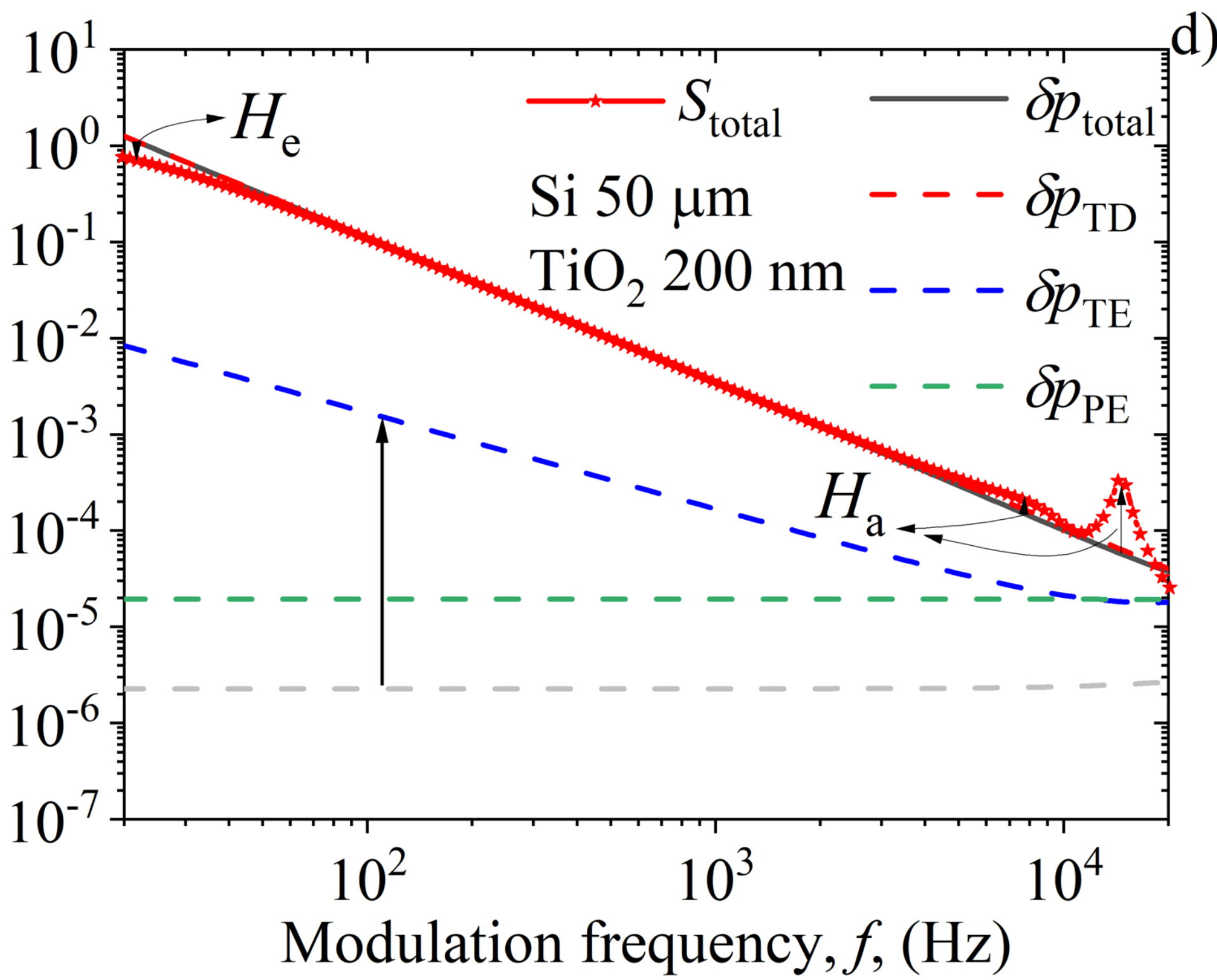
This is the author's peer reviewed, accepted manuscript. However, the online version of record will be different from this version once it has been copyedited and typeset.
PLEASE CITE THIS ARTICLE AS DOI: 10.1063/5.0079902

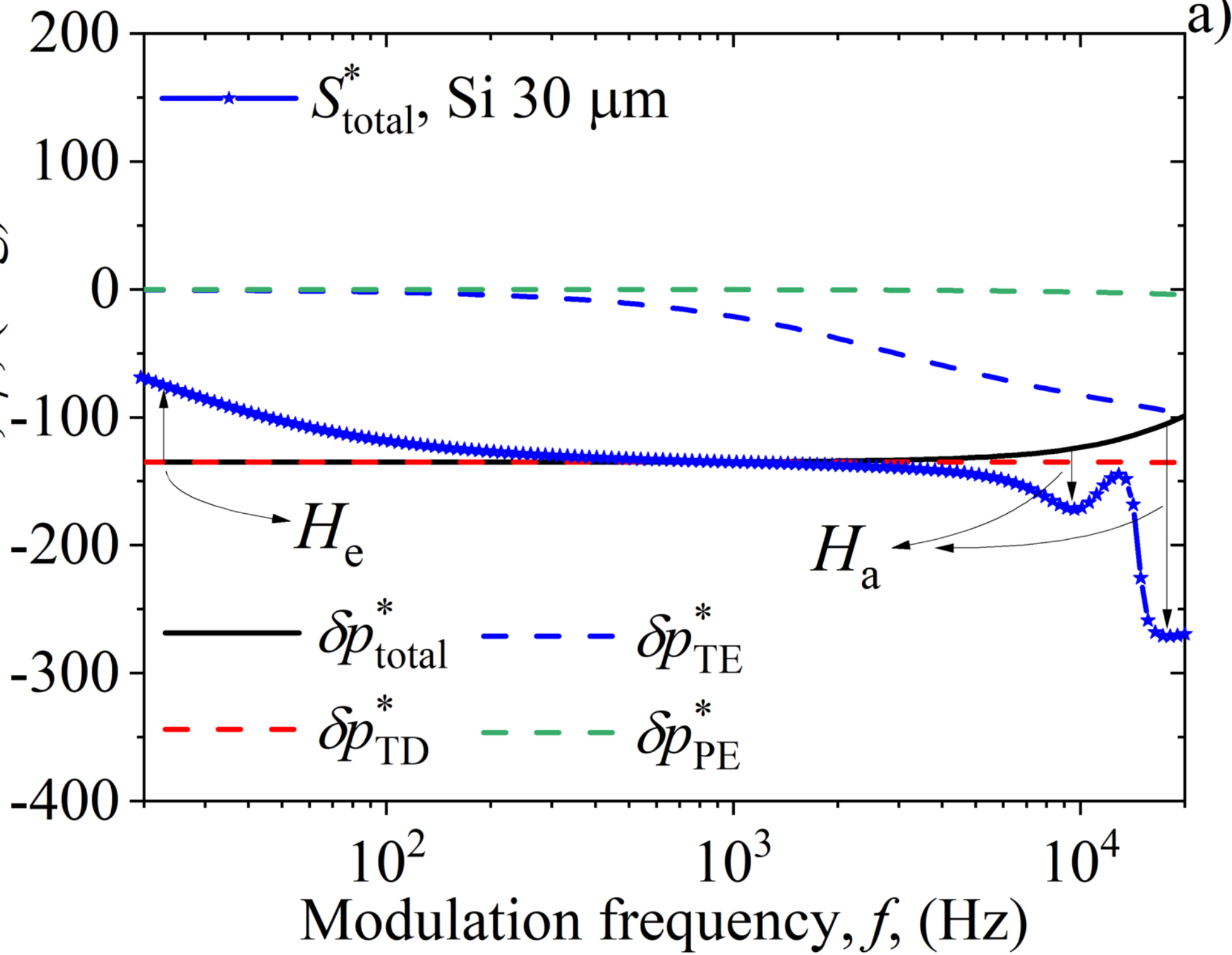
Amplitude, A , (a.u.)



This is the author's peer reviewed, accepted manuscript. However, the online version of record will be different from this version once it has been copyedited and typeset.
PLEASE CITE THIS ARTICLE AS DOI: 10.1063/5.0179902

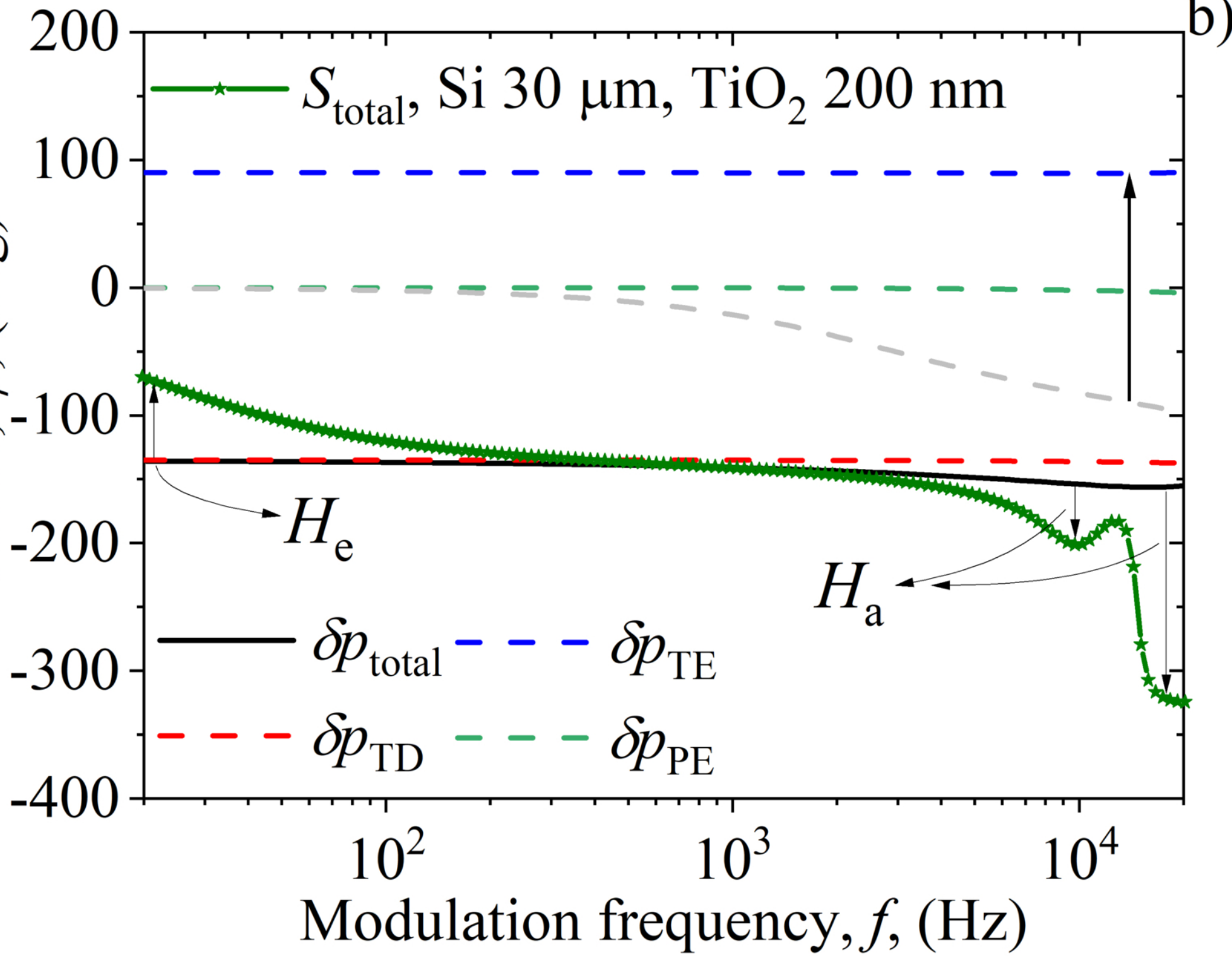
Amplitude, A , (a.u.)



Phase, φ , (deg)

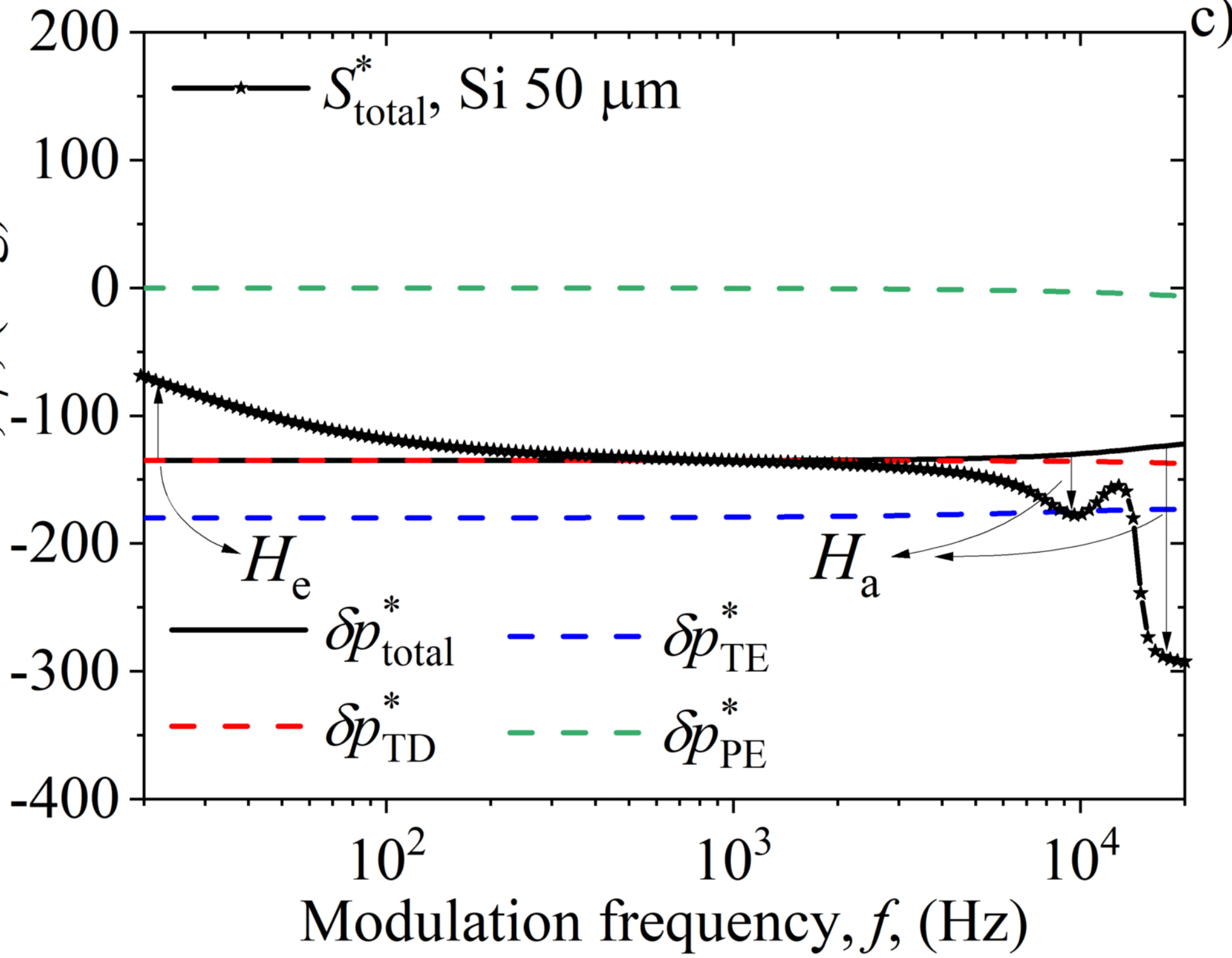
This is the author's peer reviewed, accepted manuscript. However, the online version of record will be different from this version once it has been copyedited and typeset.
PLEASE CITE THIS ARTICLE AS DOI: 10.1063/1.5007992

Phase, φ , (deg)



This is the author's peer reviewed, accepted manuscript. However, the online version of record will be different from this version once it has been copyedited and typeset.
PLEASE CITE THIS ARTICLE AS DOI: 10.1063/1.50079902

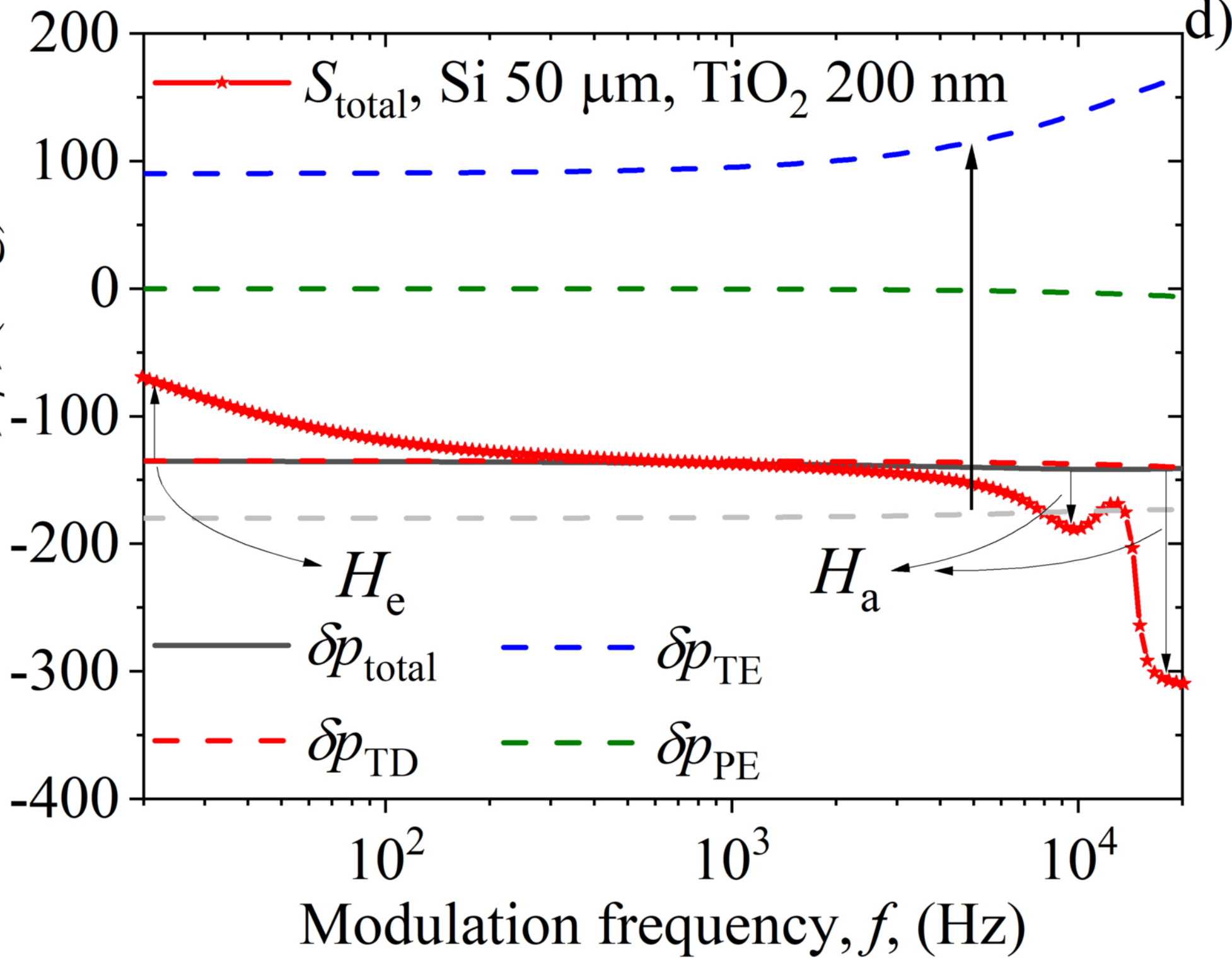
Phase, φ , (deg)



c)

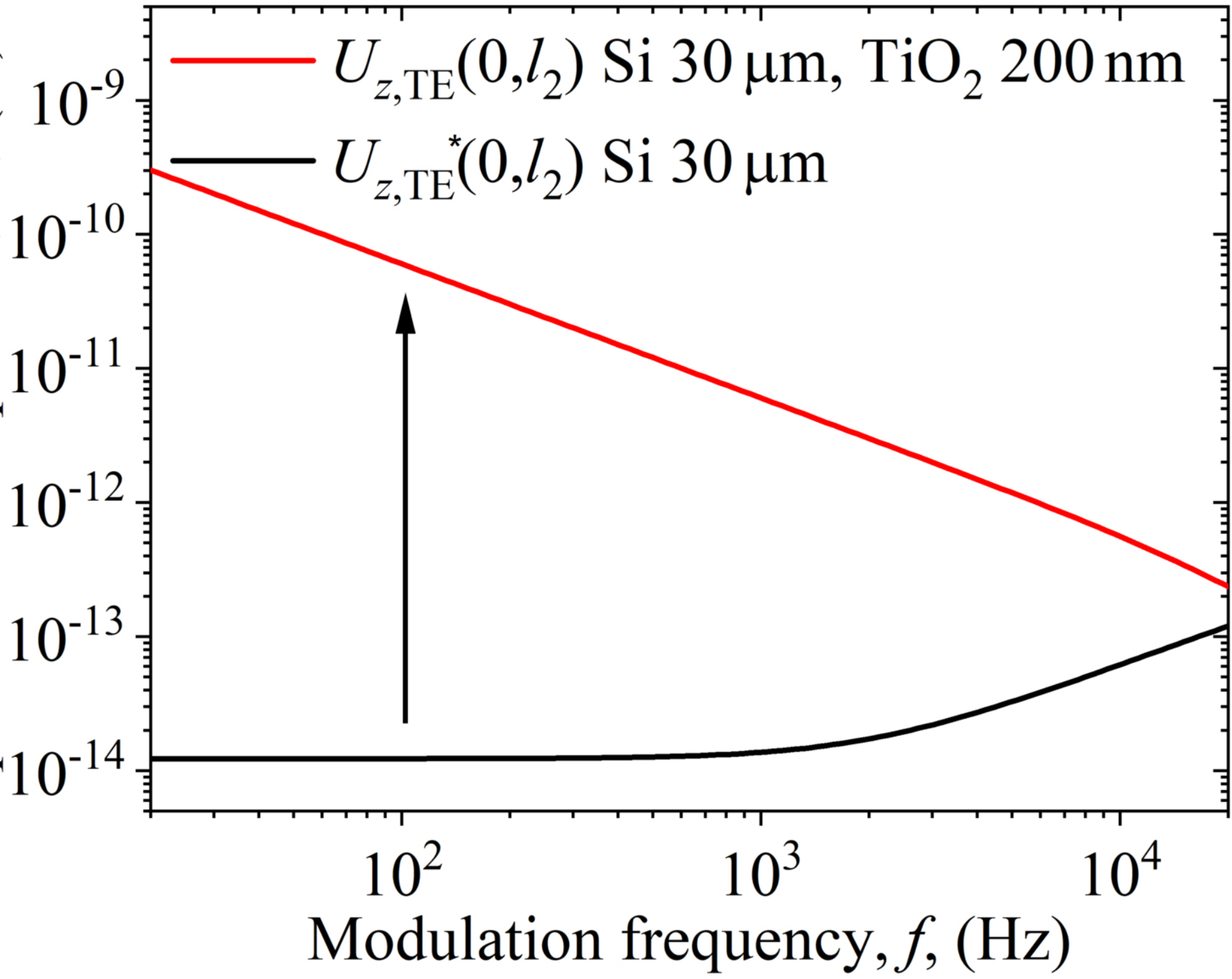
This is the author's peer reviewed, accepted manuscript. However, the online version of record will be different from this version once it has been copyedited and typeset.
PLEASE CITE THIS ARTICLE AS DOI: 10.1063/1.5007990

Phase, φ , (deg)



This is the author's peer reviewed, accepted manuscript. However, the online version of record will be different from this version once it has been copyedited and typeset.
PLEASE CITE THIS ARTICLE AS DOI: 10.1063/5.0079902

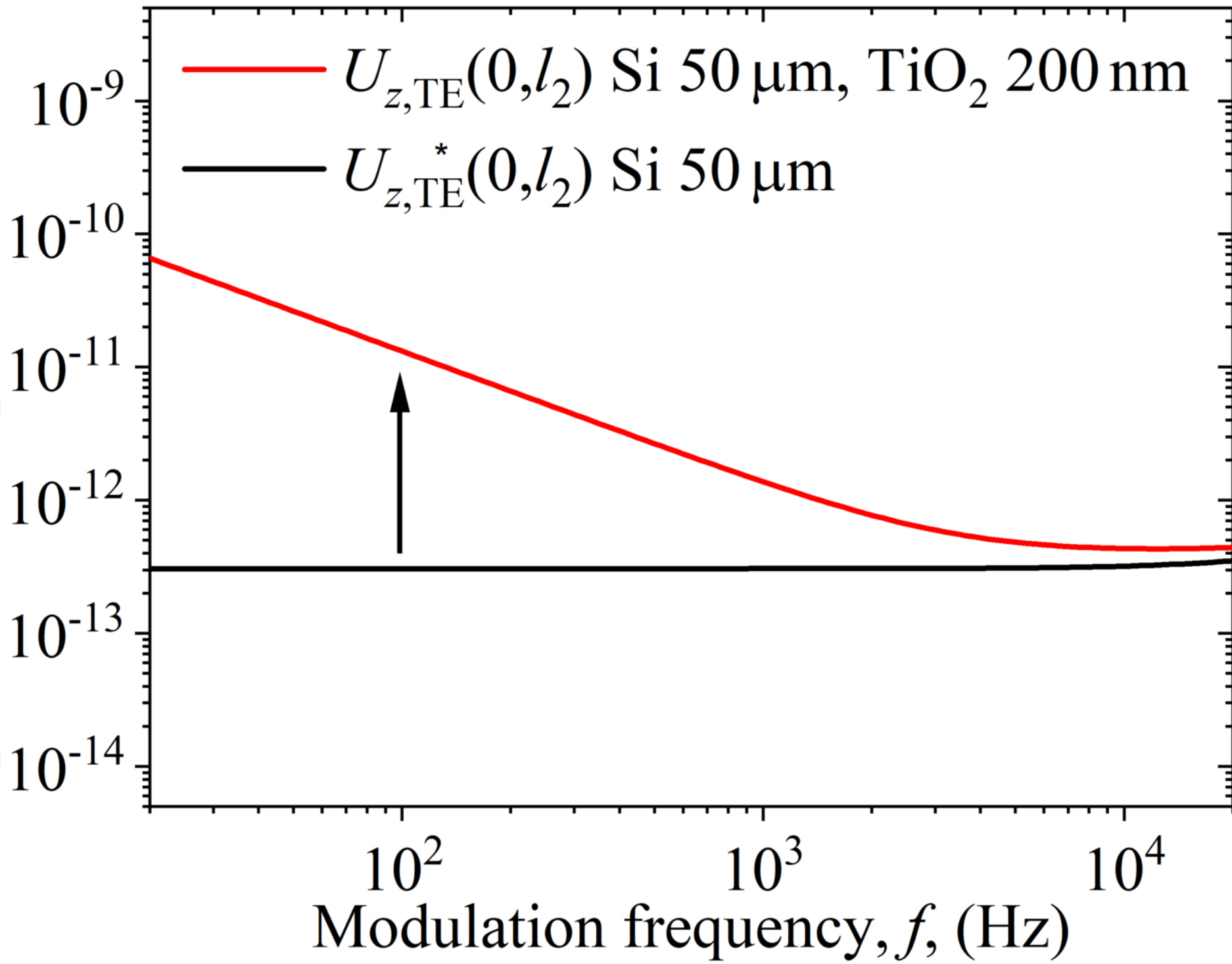
Displacement amplitude, U , (m)



a)

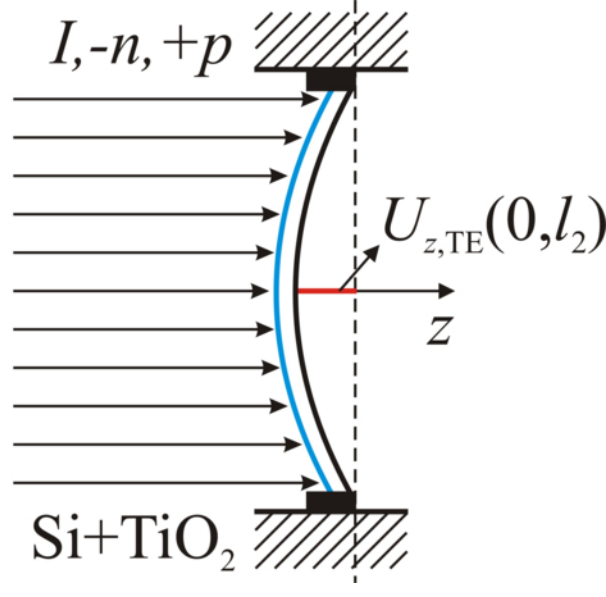
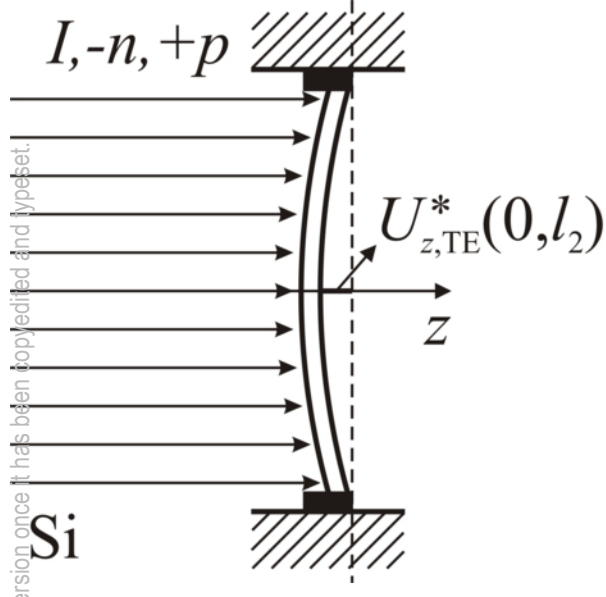
This is the author's peer reviewed, accepted manuscript. However, the online version of record will be different from this version once it has been copyedited and typeset.

PLEASE SCROLL DOWN THIS PAGE TO VIEW THE CONTENTS OF THIS MANUSCRIPT
Displacement amplitude, U , (m)

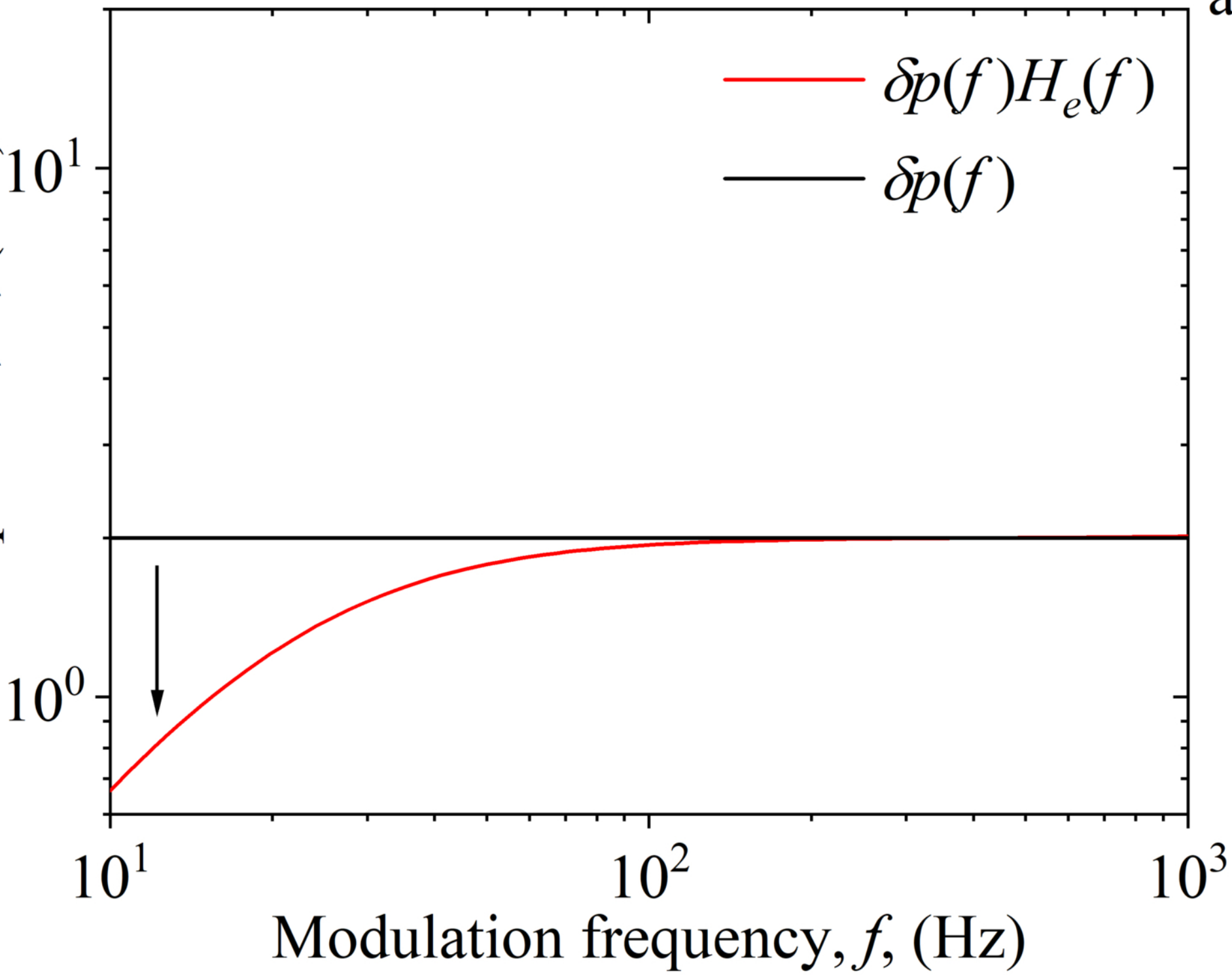


b)

This is the author's peer reviewed, accepted manuscript. However, the online version of record will be different from this version once it has been copyedited and typeset.
PLEASE CITE THIS ARTICLE AS DOI: 10.1063/5.0079902



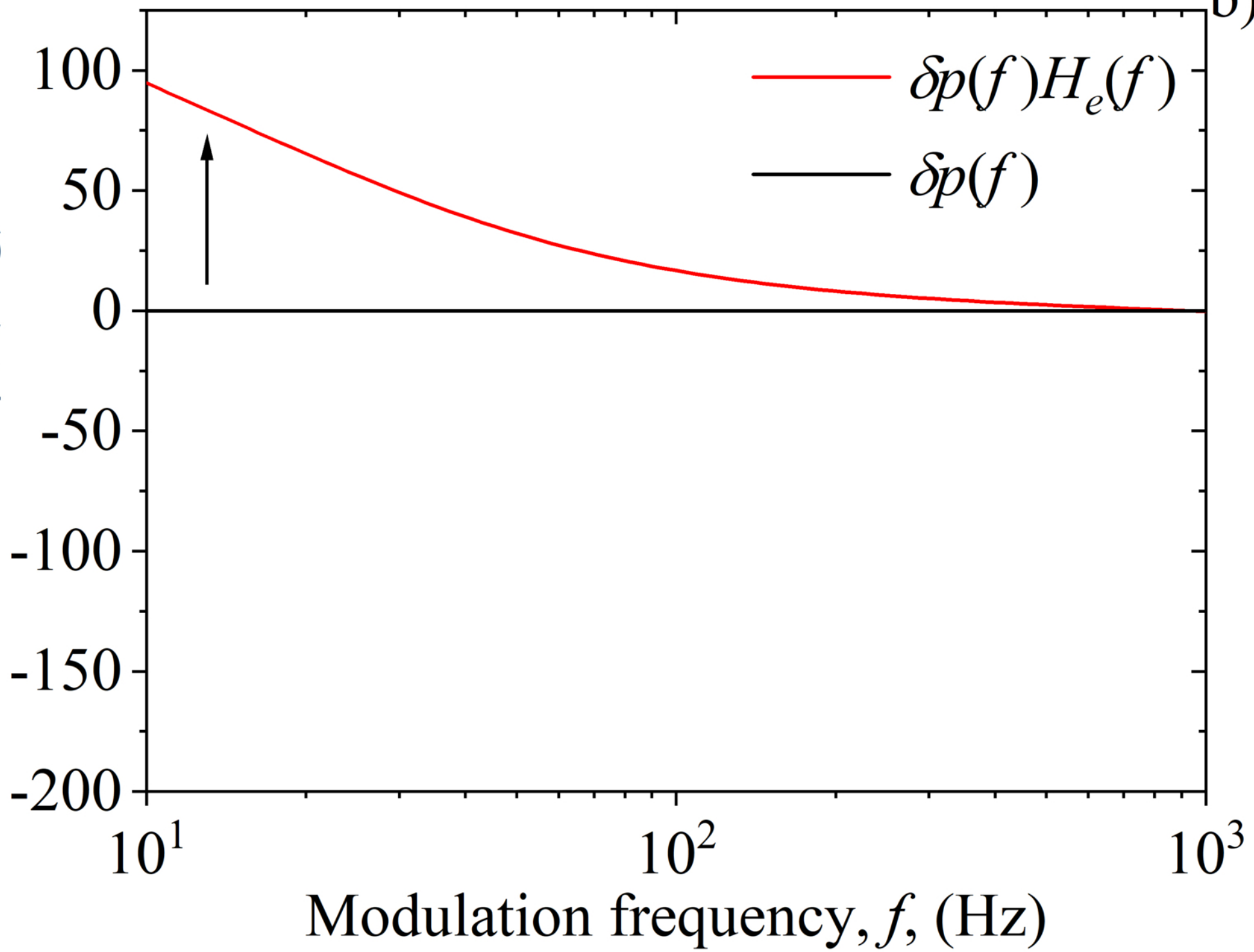
This is the author's peer reviewed, accepted manuscript. However, the online version of record will be different from this version once it has been copyedited and typeset.
PLEASE CITE THIS ARTICLE AS DOI: 10.1063/5.0079902

Amplitude, A , (a.u.)

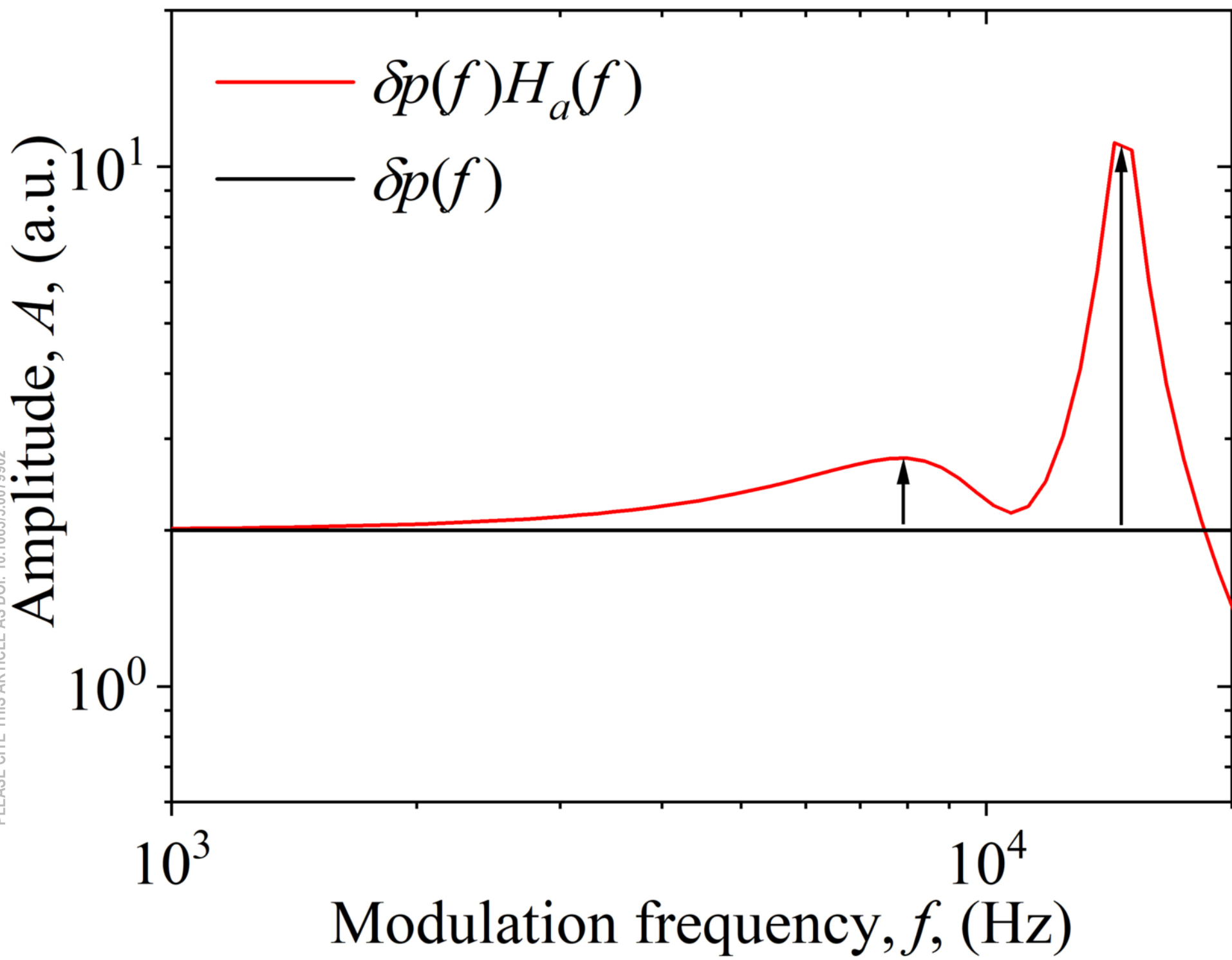
a)

This is the author's peer reviewed, accepted manuscript. However, the online version of record will be different from this version once it has been copyedited and typeset.
PLEASE CITE THIS ARTICLE AS DOI: 10.1063/1.5007892

Phase, φ , (deg)



This is the author's peer reviewed, accepted manuscript. However, the online version of record will be different from this version once it has been copyedited and typeset.
PLEASE CITE THIS ARTICLE AS DOI: 10.1063/5.0079902



This is the author's peer reviewed, accepted manuscript. However, the online version of record will be different from this version once it has been copyedited and typeset.
PLEASE CITE THIS ARTICLE AS DOI: 10.1063/1.5007892

Phase, φ , (deg)

